Masterarbeit

Zur Erlangung des akademischen Grades Master of Science

Efficient Screening in Many-Body Calculations for Low-Dimensional Materials

Eingereicht von: Ben Alex

Gutachter/innen: Prof. Dr. Claudia Draxl
PD Dr. Denis Usvyat

Eingereicht am Institut für Physik der Humboldt-Universität zu Berlin am:

Contents

1 Introduction

In recent years, low-dimensional materials have garnered significant attention in the field of condensed matter physics and materials science due to their unique electronic, optical, and mechanical properties, which set them apart from their bulk counterparts. This thesis primarily focuses on two-dimensional (2D) and one-dimensional (1D) materials. We are particularly interested in describing their electronic and optical properties. Nowadays, the gold standard for obtaining these properties is to employ many-body perturbation theory (MBPT). Specifically, the *GW* approximation for electronic structure and the Bethe-Salpeter equation (BSE) for optical properties have proven to be very reliable tools. Both methods are implemented in the all-electron full-potential code `exciting` [1]. However, when applied to low-dimensional materials, these methods can have significant shortcomings. Problems arise due to the need to simulate low-dimensional structures within a three-dimensional periodic computer code. In the case of two-dimensional materials, this involves considering periodically repeated layers, while in one-dimensional materials, periodically repeated wires must be taken into account.

The calculation of optoelectronic properties within MBPT, therefore, requires the introduction of a cutoff [2] for the Coulomb potential, as the layers or wires would otherwise interact with each other. A key ingredient for *GW* as well as BSE calculations is the screened Coulomb potential, which depends on the inverse dielectric function. The introduction of the cutoff leads to a stronger $\mathbf{q}$ dependence of the dielectric function around $\mathbf{q} = \mathbf{0}$, which requires a special treatment of the screened Coulomb potential in this region. This problem was already addressed in Ref. [2] by introducing a model function with a free parameter for the screened Coulomb potential. However, this approach was not fully *ab initio*. On the other hand, in the `exciting` code, the $\mathbf{q} = \mathbf{0}$ contribution of the screened potential was neglected. Even though it leads to the exact result, this approach requires a much denser sampling of the first Brillouin zone to capture the long-wavelength contributions of the screened potential.

In another work [3], new analytical formulas for the plane-wave matrix elements of the

screened potential were derived with *ab initio* methods in the limit $\mathbf{q} \to \mathbf{0}$. These expressions are then integrated numerically in a small region around $\mathbf{q} = \mathbf{0}$, accounting for the stronger $\mathbf{q}$ dependence of the dielectric function. For this method, a significant computational speedup was documented, compared to the approach, where the $\mathbf{q} = \mathbf{0}$ contribution is completely left out. However, these formulas were only derived for the case of a 2D cutoff and only applied to the *GW* approximation but not the BSE.

Within this thesis the approach from Ref. [3] is implemented in the `exciting` code. The first goal is to implement this procedure for the *GW* method with a 2D cutoff, intending to reproduce the results from Ref. [3]. Here, it is important to consider that in the `exciting` implementation of the *GW* approximation, the so-called product basis is used instead of plane waves. The subsequent goal is to extend the original work by demonstrating the derivation of analogous formulas for a 1D cutoff and investigating their performance in the *GW* approximation. In the final step, the analytic expressions of the screened potential for both 2D and 1D cutoffs are implemented into the BSE. This is more straightforward than for the *GW* approximation, as the BSE is already implemented in a plane wave basis.

2 Theoretical Foundations

In this chapter, we briefly outline the fundamental principles of the electronic structure problem, mainly following Ref. [4]. In the Born-Oppenheimer approximation, the electronic Hamiltonian can be written as

$$\hat{H} = \hat{T}_e + \hat{V}_{en} + \hat{V}_{ee}, \tag{2.1}$$

with

$$\hat{T}_e = -\frac{1}{2}\sum_i \nabla_i^2, \tag{2.2}$$

$$\hat{V}_{en} = -\sum_{i,I} \frac{Z_I}{|\mathbf{r}_i - \mathbf{R}_I|}, \tag{2.3}$$

$$\hat{V}_{ee} = \frac{1}{2}\sum_{i\neq j} \frac{1}{|\mathbf{r}_i - \mathbf{r}_j|}. \tag{2.4}$$

Here, small coordinates and indices $\mathbf{r}_i$ represent electrons, while capital coordinates $\mathbf{R}_I$ represent the nuclei of the system. The Z_I are the charge numbers of the corresponding nuclei. Throughout this thesis, we use atomic units, where

$$\hbar = m_e = e = \frac{4\pi}{\epsilon_0} = 1. \tag{2.5}$$

2.1 Density Functional Theory

The foundation of density function theory (DFT) lies in the Hohenberg-Kohn theorems, which state that the ground-state electron density $\rho(\mathbf{r})$ uniquely determines the external potential and the total energy of a system. The total energy functional, denoted as $E[\rho]$,

can be expressed as the sum of various terms

$$E[\rho] = T_0[\rho] + E_{\text{ext}}[\rho] + E_H[\rho] + E_{xc}[\rho]. \tag{2.6}$$

Here, $T_0[\rho]$ represents the independent particle kinetic energy, $E_{\text{ext}}[\rho]$ is the external potential energy, $E_H[\rho]$ corresponds to the Hartree energy, and $E_{xc}[\rho]$ is the exchange-correlation energy. The Kohn-Sham approach is to introduce a fictitious system of non-interacting particles, which has the same density as the original system. Then, the density is expressed as a summation over all occupied orbitals

$$\rho(\mathbf{r}) = \sum_{n\mathbf{k}} f_{n\mathbf{k}} |\psi_{n\mathbf{k}}(\mathbf{r})|^2, \tag{2.7}$$

where $\psi_{n\mathbf{k}}(\mathbf{r})$ are the wavefunctions of the non-interacting particles and $f_{n\mathbf{k}}$ are the occupation numbers. The Bloch wavevector $\mathbf{k}$ accounts for the translational symmetry and lies within the first Brillouin zone (BZ). The wavefunctions can be obtained by diagonalizing the Kohn-Sham Hamiltonian $h_{KS}(\mathbf{r})$

$$h_{KS}(\mathbf{r})\psi_{n\mathbf{k}}(\mathbf{r}) = \epsilon_{n\mathbf{k}}\psi_{n\mathbf{k}}(\mathbf{r}), \tag{2.8}$$

with corresponding eigenvalues $\epsilon_{n\mathbf{k}}$. An expression for the Kohn-Sham Hamiltonian can be obtained by minimizing the functional in Eq. 2.6 with respect to the electron density. The final expression is

$$h_{KS}(\mathbf{r}) = -\frac{1}{2}\nabla^2 + v_{\text{ext}}(\mathbf{r}) + v_H(\mathbf{r}, [\rho]) + v_{xc}(\mathbf{r}, [\rho]). \tag{2.9}$$

Here, $v_{\text{ext}}(\mathbf{r})$ represents the external potential, $v_H(\mathbf{r}, [\rho])$ is the Hartree potential, and $v_{xc}(\mathbf{r}, [\rho])$ is the exchange-correlation potential. The external potential $v_{ext}(\mathbf{r})$ accounts for the interaction between electrons and external sources. The Hartree potential $v_H(\mathbf{r})$ is defined as

$$v_H(\mathbf{r}) = \int \frac{\rho(\mathbf{r}')}{|\mathbf{r} - \mathbf{r}'|}\, \mathrm{d}\mathbf{r}'. \tag{2.10}$$

For the exchange correlation potential $v_{xc}(\mathbf{r})$ one needs to make appropriate approximations, which are not discussed in detail here. The eigenvalues obtained by solving the Kohn-Sham equations cannot be interpreted as electron addition or removal energies.

However, they serve as a good starting point for more elaborate methods which will be described in the next section.

2.2 Many-Body Perturbation Theory

2.2.1 Quasi-particles and One Particle Green's Functions

The idea behind the introduction of quasi-particles (QP) is to construct particles, that extend beyond the scope of non-interacting particles in theories such as Kohn-Sham theory. Quasi-particles are defined as particles dressed with their interactions with other particles. Hence, they have effective properties which account for many-body correlation effects of a system of interacting particles. Overall, they have modified energies and lifetimes, while still maintaining the same quantum numbers as the non-interacting particles.

The Green's function is a powerful tool to describe quasi-particles in many-body perturbation theory (MBPT). It can be defined for a system of quasi-particles and it contains important information about the system. It can be interpreted as a propagator, containing the probability of a particle propagating from $\mathbf{r}_1$ at time t_1 to $\mathbf{r}_2$ at time t_2. When performing a Fourier transform to frequency space, it can be shown that the Green's function has poles at the eigenvalues of the system. One can derive the so-called Dyson equation, that relates the Green's function of the interacting system G with the Green's function of the non-interacting system G_0

$$G(1,2) = G_0(1,2) + \int G_0(1,3)\Sigma(3,4)G(4,2)\mathrm{d}(3,4). \tag{2.11}$$

Here, we introduced the notation

$$1 \equiv (\mathbf{r}_1, t_1), \tag{2.12}$$

$$\mathrm{d}1 \equiv \mathrm{d}\mathbf{r_1}\mathrm{d}t_1. \tag{2.13}$$

The self-energy Σ represents the effects of interactions between quasi-particles. It includes contributions from all possible interactions within the system. Using the Dyson

equation, one can derive the so-called quasi-particle equation

$$\left[-\frac{1}{2}\nabla^2 + v_{\text{ext}}(\mathbf{r}) + v_H(\mathbf{r})\right]\Psi_{n\mathbf{k}}(\mathbf{r}) + \int \Sigma\left(\mathbf{r}, \mathbf{r}'; E^{\text{qp}}_{n\mathbf{k}}\right)\Psi_{n\mathbf{k}}\left(\mathbf{r}'\right)\mathrm{d}\mathbf{r}' = E^{\text{qp}}_{n\mathbf{k}}\Psi_{n\mathbf{k}}(\mathbf{r}). \quad 2.14$$

This equation looks like a Schrödinger equation for quasi-particles, but it is important to note that the self-energy is a non-hermitian operator. This results in complex eigenvalues $E^{\text{qp}}_{n\mathbf{k}}$. The real part of the eigenvalues then corresponds to the quasi-particle energy, while the imaginary part can be related to the lifetime. Furthermore, the self-energy is non-local and its dependence on the eigenvalues $E_{n\mathbf{k}}$ makes Eq. 2.14 non-linear. Therefore, it is very complicated to solve this equation.

2.2.2 Hedin Equations and the GW Approach

In order to calculate the self-energy, Hedin originally derived [5, 6] the following coupled equations

$$\Sigma(1,2) = i\int G(1,4)W(1,3)\Gamma(4,2;3)\mathrm{d}(3,4), \quad 2.15$$

$$W(1,2) = v(1,2) + \int v(1,3)\hat{P}(3,4)W(4,2)\mathrm{d}(3,4), \quad 2.16$$

$$\hat{P}(1,2) = -i\int G(1,3)G(4,1)\Gamma(3,4;2)\mathrm{d}(3,4), \quad 2.17$$

$$\Gamma(1,2;3) = \delta(1,2)\delta(1,3) + \int \frac{\delta\Sigma(1,2)}{\delta G(4,5)}G(4,6)G(7,5)\Gamma(6,7;3)\mathrm{d}(4,5,6,7). \quad 2.18$$

Here, $\hat{P}$ is the irreducible polarizability, Γ the vertex function, and W the screened interaction. The bare Coulomb potential $v(1,2)$ reads

$$v(1,2) \equiv \frac{1}{|\mathbf{r}_1 - \mathbf{r}_2|}\delta(t_1 - t_2). \quad 2.19$$

Solving Hedin's equations is a very complex task since they are coupled to each other, requiring iterative solutions. To simplify the complexity of the task, one common approximation neglects the second contribution to the vertex function in Eq. 2.18. This leads to the following simplified equations

$$\Sigma(1,2) = iG(1,2)W(1,2), \tag{2.20}$$

$$W(1,2) = v(1,2) + \int v(1,3)\hat{P}(3,4)W(4,2)\mathrm{d}(3,4), \tag{2.21}$$

$$\hat{P}(1,2) = -iG(1,2)G(2,1), \tag{2.22}$$

$$\Gamma(1,2;3) = \delta(1,2)\delta(1,3). \tag{2.23}$$

When neglecting vertex corrections to the polarizability, one often speaks of the random phase approximation (RPA). The simplified expression for the self-energy Σ in Eq. 2.20 gives the GW approximation its name, since the self-energy is now computed as a product of Green's function and screened interaction. Furthermore, we can now introduce the dielectric function as

$$\varepsilon(1,2) = \delta(1,2) - \int v(1,3)\hat{P}(3,2)\mathrm{d}(3), \tag{2.24}$$

which allows solving the integral equation for the screened interaction W using its inverse

$$W(1,2) = \int \varepsilon^{-1}(1,3)v(3,2)\mathrm{d}(3). \tag{2.25}$$

By performing a Fourier transform to frequency space and writing the $\mathbf{r}$ coordinates explicitly, one gets following expressions as a starting point

$$\Sigma\left(\mathbf{r},\mathbf{r}';\omega\right) = \frac{i}{2\pi}\int G\left(\mathbf{r},\mathbf{r}';\omega+\omega'\right)W\left(\mathbf{r}',\mathbf{r};\omega'\right)e^{i\omega'\eta}\mathrm{d}\omega', \tag{2.26}$$

$$W\left(\mathbf{r},\mathbf{r}';\omega\right) = \int \varepsilon^{-1}\left(\mathbf{r},\mathbf{r}_1;\omega\right)v\left(\mathbf{r}_1,\mathbf{r}'\right)\mathrm{d}\mathbf{r}_1, \tag{2.27}$$

$$\varepsilon\left(\mathbf{r},\mathbf{r}';\omega\right) = \delta\left(\mathbf{r},\mathbf{r}'\right) - \int v\left(\mathbf{r},\mathbf{r}_1\right)\hat{P}\left(\mathbf{r}_1,\mathbf{r}';\omega\right)\mathrm{d}\mathbf{r}_1, \tag{2.28}$$

$$\hat{P}\left(\mathbf{r},\mathbf{r}';\omega\right) = -\frac{i}{2\pi}\int G\left(\mathbf{r},\mathbf{r}';\omega+\omega'\right)G\left(\mathbf{r}',\mathbf{r};\omega'\right)e^{i\omega'\eta}\mathrm{d}\omega'. \tag{2.29}$$

The G_0W_0 approximation

In `exciting` [1, 7] first order perturbation theory is applied to simplify the solution of Eq. 2.26 to Eq. 2.29. The common choice for the non-interacting system is the

solution of the Kohn-Sham equation. It can be argued [8] that the wavefunctions of the Kohn-Sham system, denoted as $\psi_{n\mathbf{k}}$, are a good approximation to their quasi-particle counterparts $\Psi_{n\mathbf{k}}$. By inserting the Kohn-Sham wavefunctions into the quasi-particle equation Eq. 2.14, we obtain the following simplified expression for the real parts of the quasi-particle energies $\epsilon^{\mathrm{qp}}_{n\mathbf{k}} \equiv \mathrm{Re}\,(E^{\mathrm{qp}}_{n\mathbf{k}})$

$$\epsilon^{\mathrm{qp}}_{n\mathbf{k}} = \epsilon_{n\mathbf{k}} + \langle \psi_{n\mathbf{k}}(\mathbf{r}) \left| \mathrm{Re}\left[\Sigma\left(\mathbf{r},\mathbf{r}';\epsilon^{\mathrm{qp}}_{n\mathbf{k}}\right)\right] - v_{xc}(\mathbf{r})\delta\left(\mathbf{r}-\mathbf{r}'\right)\right| \psi_{n\mathbf{k}}\left(\mathbf{r}'\right)\rangle\,. \tag{2.30}$$

Introducing a shorthand notation, we can write the energies as

$$\epsilon^{\mathrm{qp}}_{n\mathbf{k}} = \epsilon_{n\mathbf{k}} + \mathrm{Re}\,\Sigma_{n\mathbf{k}}\left(\epsilon^{\mathrm{qp}}_{n\mathbf{k}}\right) - v_{xc,n\mathbf{k}}. \tag{2.31}$$

Here, the quasi-particle energy $\epsilon^{\mathrm{qp}}_{n\mathbf{k}}$ still appears on both sides of the equation. Hence, we expand the self-energy around $\epsilon_{n\mathbf{k}}$

$$\mathrm{Re}\,\Sigma_{n\mathbf{k}}\left(\epsilon^{\mathrm{qp}}_{n\mathbf{k}}\right) = \mathrm{Re}\,\Sigma_{n\mathbf{k}}\left(\epsilon_{n\mathbf{k}}\right) + \left(\frac{\partial}{\partial\omega}\,\mathrm{Re}\,\Sigma_{n\mathbf{k}}(\omega)\right)_{\omega=\epsilon_{n\mathbf{k}}} \left(\epsilon^{\mathrm{qp}}_{n\mathbf{k}} - \epsilon_{n\mathbf{k}}\right). \tag{2.32}$$

Inserting the expansion from Eq. 2.32 in Eq. 2.31, we arrive at following equation

$$\epsilon^{\mathrm{qp}}_{n\mathbf{k}} = \epsilon_{n\mathbf{k}} + Z_{n\mathbf{k}}\left[\mathrm{Re}\,\Sigma_{n\mathbf{k}}\left(\epsilon_{n\mathbf{k}}\right) - v_{xc,n\mathbf{k}}\right], \tag{2.33}$$

where we have introduced the quasi-particle renormalization factor

$$Z_{n\mathbf{k}} = \left[1 - \left(\frac{\partial}{\partial\omega}\,\mathrm{Re}\,\Sigma^{c}_{n\mathbf{k}}(\omega)\right)_{\omega=\epsilon_{n\mathbf{k}}}\right]^{-1}. \tag{2.34}$$

Now, we discuss how to obtain the real space representation of the self-energy. For the Green's function, we use the non-interacting counterpart, obtained from solving the Kohn-Sham equations

$$G_0\left(\mathbf{r},\mathbf{r}';\omega\right) = \sum_{n\mathbf{k}} \frac{\psi_{n\mathbf{k}}(\mathbf{r})\psi^{*}_{n\mathbf{k}}\left(\mathbf{r}'\right)}{\omega - \tilde{\epsilon}_{n\mathbf{k}}}, \tag{2.35}$$

with

$$\tilde{\epsilon}_{n\mathbf{k}} \equiv \epsilon_{n\mathbf{k}} + i\eta \,\mathrm{sgn}\left(\epsilon_F - \epsilon_{n\mathbf{k}}\right). \tag{2.36}$$

We obtain the polarizability by inserting the non-interacting Green's function in Eq. 2.29

$$\begin{aligned}\hat{P}_0(\mathbf{r},\mathbf{r}';\omega) = -\frac{i}{\pi}\sum_{n\mathbf{k}}\sum_{m\mathbf{k}'}\psi_{n\mathbf{k}}(\mathbf{r})\psi^*_{n\mathbf{k}}(\mathbf{r}')\psi_{m\mathbf{k}'}(\mathbf{r}')\psi^*_{m\mathbf{k}'}(\mathbf{r}) \\ \cdot\int \frac{e^{i\omega'\eta}}{(\omega-\tilde{\epsilon}_{n\mathbf{k}}+\omega')(\omega'-\tilde{\epsilon}_{m\mathbf{k}'})}\,\mathrm{d}\omega',\end{aligned} \tag{2.37}$$

where spins have been summed, accounting for an additional factor 2. The remaining frequency integral can be calculated to be[7]

$$\begin{aligned}F_{nm}(\mathbf{k},\mathbf{q};\omega) &\equiv -\frac{i}{\pi}\int \frac{e^{i\omega'\eta}}{(\omega-\tilde{\epsilon}_{n\mathbf{k}}+\omega')(\omega'-\tilde{\epsilon}_{m\mathbf{k}-\mathbf{q}})}\,\mathrm{d}\omega' \\ &= 2f_{n\mathbf{k}}\left(1-f_{m\mathbf{k}-\mathbf{q}}\right)\left\{\frac{1}{\omega-\epsilon_{m\mathbf{k}-\mathbf{q}}+\epsilon_{n\mathbf{k}}+i\eta} - \frac{1}{\omega+\epsilon_{m\mathbf{k}-\mathbf{q}}-\epsilon_{n\mathbf{k}}-i\eta}\right\}.\end{aligned} \tag{2.38}$$

The occupation numbers $f_{n\mathbf{k}}$ arise, because the poles only contribute to the integral, when one is in the upper and the other in the lower complex plane. This situation corresponds to having one occupied and one unoccupied state, cf. Eq. 2.36. Otherwise, their contributions to the integral cancel. We also introduced the vector $\mathbf{q} = \mathbf{k} - \mathbf{k}'$, to rewrite the dependence on $\mathbf{k}'$. Overall, the final expression for the polarizability reads

$$\hat{P}_0\left(\mathbf{r},\mathbf{r}';\omega\right) = \sum_{n,m}\sum_{\mathbf{k},\mathbf{q}} F_{nm}(\mathbf{k},\mathbf{q};\omega)\psi_{n\mathbf{k}}(\mathbf{r})\psi^*_{m\mathbf{k}-\mathbf{q}}(\mathbf{r})\psi^*_{n\mathbf{k}}\left(\mathbf{r}'\right)\psi_{m\mathbf{k}-\mathbf{q}}\left(\mathbf{r}'\right). \tag{2.39}$$

One can then insert the polarizability in Eq. 2.28 to obtain the dielectric function ε. By inverting the dielectric function, one can utilize Eq. 2.27 to arrive at an expression for the screened interaction W_0. In the context of GW calculations, one often defines a correlation part of the screened potential by subtracting the bare Coulomb potential

$$W_0^c\left(\mathbf{r},\mathbf{r}';\omega\right) = W_0\left(\mathbf{r},\mathbf{r}';\omega\right) - v\left(\mathbf{r},\mathbf{r}'\right). \tag{2.40}$$

Then, the correlation part of the self-energy is defined by inserting the correlation part of the screened potential in Eq. 2.26

$$\begin{aligned}\Sigma^c(\mathbf{r},\mathbf{r}';\omega) &= \frac{i}{2\pi}\int G_0(\mathbf{r},\mathbf{r}';\omega+\omega')\,W_0^c(\mathbf{r}',\mathbf{r};\omega')\,\mathrm{d}\omega' \\ &= \sum_{n\mathbf{k}}\psi_{n\mathbf{k}}(\mathbf{r})\psi^*_{n\mathbf{k}}(\mathbf{r}')\int\frac{W_0^c(\mathbf{r}',\mathbf{r};\omega')}{\omega+\omega'-\tilde{\epsilon}_{n\mathbf{k}}}\mathrm{d}\omega'. \end{aligned} \tag{2.41}$$

The remaining frequency integral cannot be simplified further and has to be evaluated numerically. Finally, the exchange part of the self-energy is obtained by inserting the bare Coulomb potential in Eq. 2.26

$$\begin{aligned}\Sigma^x(\mathbf{r},\mathbf{r}') &= \frac{i}{2\pi}\int G_0(\mathbf{r},\mathbf{r}';\omega')\,v(\mathbf{r}',\mathbf{r})\,e^{i\omega'\eta}\mathrm{d}\omega' \\ &= -\sum_{n\mathbf{k}} f_{n\mathbf{k}}\psi_{n\mathbf{k}}(\mathbf{r})v(\mathbf{r}',\mathbf{r})\,\psi^*_{n\mathbf{k}}(\mathbf{r}')\,. \end{aligned} \tag{2.42}$$

2.2.3 The Bethe Salpeter Equation

So far, we have described the one-particle excitation energies of electronic systems. Now we want to shift the focus on describing optical properties of the system, where we follow Refs. [4, 9]. In order to understand these properties correctly, it is important to realize that photons can create electron-hole pairs. One is especially interested in excitons, which are defined as bound electron-hole pairs with the lowest energies below the band gap. Electron-hole pairs are formally described by using the two-particle Green's function G_2. The two-particle correlation function can be defined as

$$L(1,1',2,2') = G_2(1,1',2,2') - G(1',2')G(1,2). \tag{2.43}$$

It is possible to derive the Bethe-Salpeter equation for this correlation function L

$$\begin{aligned}L(1,1',2,2') &= L_0(1,1',2,2') \\ &\quad + \int \mathrm{d}(3,3',4,4')\,L_0(1,1',3,3')\,\Xi(3,3',4,4')\,L(4,4',2,2')\,. \end{aligned} \tag{2.44}$$

Here, Ξ is the interaction kernel, which is defined as the functional derivative of the self-energy Σ with respect to the one-particle Green's function

$$\Xi\left(3,3',4,4'\right) = -i\delta\left(3,3'\right)\delta\left(4,4'\right)v(3,4) + \frac{\delta\Sigma\left(4,4'\right)}{\delta G\left(3,3'\right)}. \tag{2.45}$$

Furthermore, we introduced the quantity L_0, which describes the independent motion of two particles

$$L_0\left(1,1',2,2'\right) = G\left(1',2'\right)G(2,1). \tag{2.46}$$

From the solution of the BSE the complete polarizability P can be obtained via the relation

$$P(1,2) = -iL(1,1,2,2). \tag{2.47}$$

The BSE in the GW Approximation

In order to solve the BSE, we need an approximation for the interaction kernel defined in Eq. 2.45. We have previously discussed that the self-energy can be calculated in the GW approximation, as shown in Eq. 2.20. By using the GW approximation in this case, we obtain following expression for the interaction kernel

$$\begin{aligned}\Xi\left(3,3',4,4'\right) = &-i\delta\left(3,3'\right)\delta\left(4,4'\right)v(3,4) + i\delta(3,4)\delta\left(3',4'\right)W\left(3,3'\right) \\ &+ iG\left(4,4'\right)\frac{\delta W\left(4,4'\right)}{\delta G\left(3,3'\right)}.\end{aligned} \tag{2.48}$$

The only unknown in this equation is the functional derivative of W with respect to G. However, it is usually believed to contribute significantly less than the other two terms. Therefore, we neglect the term in the following. The term containing the bare Coulomb potential describes the repulsive and unscreened exchange interaction. The other term contains the screened interaction and describes the attractive electron hole interaction. So far, the BSE implicitly contains the spin coordinates. It can be demonstrated that the equation can be split up in singlet and triplet contributions. Schematically the BSE then reads

$$L^{\text{singlet}} = L_0 + iL_0\left[W - 2v\right]L^{\text{singlet}} \tag{2.49}$$

$$L^{\text{triplet}} = L_0 + iL_0WL^{\text{triplet}}\,. \tag{2.50}$$

While the Coulomb potential does not enter the triplet contribution, it contributes twice to the singlet. In this work we focus on the BSE for singlets.

The BSE Hamiltonian

In order to get a solution for the two-particle correlation function L, it is useful to reformulate the problem into an effective two-particle Schrödinger equation. To do so, we insert the independent particle Green's function from Eq. 2.35 in Eq. 2.46, perform a Fourier transform to frequency space, and find that L_0 takes following simple form in the basis of non-interacting particles

$$L^0_{i_1 i_2, i_3 i_4}(\omega) = -2i \frac{(f_{i_2} - f_{i_1})\, \delta_{i_1 i_3} \delta_{i_2 i_4}}{\epsilon_{i_2} - \epsilon_{i_1} - \omega - i\eta}. \tag{2.51}$$

Here, we introduced the short hand notation

$$i_1 = n_1 \mathbf{k}, \tag{2.52}$$
$$i_2 = n_2 \mathbf{k}, \tag{2.53}$$
$$i_3 = n_3 \mathbf{k}', \tag{2.54}$$
$$i_4 = n_4 \mathbf{k}', \tag{2.55}$$

where we have restricted ourselves to optical transitions, meaning that there is no momentum transfer between i_1 and i_2 or i_3 and i_4. The factor 2 comes from a summation over spins and the f_i are occupation numbers. The BSE can then be expanded in this basis, which yields following result

$$L_{i_1 i_2, i_3 i_4}(\omega) = \left[L_0^{-1} + \frac{i}{2} \Xi \right]^{-1}_{i_1 i_2, i_3 i_4} = 2i \left[H^{2p} - \mathbb{1} z \right]^{-1}_{i_1 i_2, i_3 i_4} (f_{i_4} - f_{i_3}). \tag{2.56}$$

with the effective two particle Hamiltonian

$$H^{2p}_{i_1 i_2, i_3 i_4} = (\epsilon_{i_2} - \epsilon_{i_1})\, \delta_{i_1 i_3} \delta_{i_2 i_4} - i\, (f_{i_2} - f_{i_1})\, \Xi_{i_1 i_2, i_3 i_4}. \tag{2.57}$$

This Hamiltonian exhibits a 2×2 block structure, when one distinguishes between resonant (i.e. from a valence state v to a conduction state c) and anti-resonant (from a conduction state c to a valence state v) transitions

$$H^{2p} = \begin{pmatrix} H^{\mathrm{rr}} & H^{\mathrm{ra}} \\ H^{\mathrm{ar}} & H^{\mathrm{aa}} \end{pmatrix}. \tag{2.58}$$

This problem can be further simplified by applying the so-called Tamm–Dancoff approximation (TDA), which neglects the coupling between resonant and anti-resonant parts. Then we just have to investigate contributions of the type

$$H^{2p}_{v_1c_1\mathbf{k}_1,v_2c_2\mathbf{k}_2} = (\epsilon_{c_1\mathbf{k}_1} - \epsilon_{v_1\mathbf{k}_1})\,\delta_{v_1v_2}\delta_{c_1c_2}\delta_{\mathbf{k}_1\mathbf{k}_2} + i\Xi_{v_1c_1\mathbf{k}_1,v_2c_2\mathbf{k}_2}. \tag{2.59}$$

We restrict ourselves to the singlet contribution and write the Hamiltonian as a sum of diagonal, exchange and direct term

$$H^{2p} = H^{\mathrm{diag}} + H^{\mathrm{x}} + H^{\mathrm{dir}}, \tag{2.60}$$

where the matrix elements are defined as

$$H^{\mathrm{diag}}_{v_1c_1\mathbf{k}_1,v_2c_2\mathbf{k}_2} = (\epsilon_{c_1\mathbf{k}_1} - \epsilon_{v_1\mathbf{k}_1})\,\delta_{v_1v_2}\delta_{c_1c_2}\delta_{\mathbf{k}_1\mathbf{k}_2} \tag{2.61}$$

$$H^{\mathrm{x}}_{v_1c_1\mathbf{k}_1,v_2c_2\mathbf{k}_2} = 2\int \mathrm{d}\mathbf{r}_1 \int \mathrm{d}\mathbf{r}_2 \psi_{v_1\mathbf{k}_1}(\mathbf{r}_1)\,\psi^*_{c_1\mathbf{k}_1}(\mathbf{r}_1)\,v(\mathbf{r}_1,\mathbf{r}_2)\,\psi^*_{v_2\mathbf{k}_2}(\mathbf{r}_2)\,\psi_{c_2\mathbf{k}_2}(\mathbf{r}_2) \tag{2.62}$$

$$H^{\mathrm{dir}}_{v_1c_1\mathbf{k}_1,v_2c_2\mathbf{k}_2} = -\int \mathrm{d}\mathbf{r}_1 \int \mathrm{d}\mathbf{r}_2 \psi_{v_1\mathbf{k}_1}(\mathbf{r}_1)\,\psi^*_{c_1\mathbf{k}_1}(\mathbf{r}_2)\,W(\mathbf{r}_1,\mathbf{r}_2)\,\psi^*_{v_2\mathbf{k}_2}(\mathbf{r}_1)\,\psi_{c_2\mathbf{k}_2}(\mathbf{r}_2). \tag{2.63}$$

In order to get an expression for L, we need to invert the matrix $[H^{2p} - \mathbb{1}z]$. This can be straightforwardly done by diagonalizing it

$$\sum_{v'c'\mathbf{k}'} H^{2p}_{vc\mathbf{k},v'c'\mathbf{k}'} A^{\lambda}_{v'c'\mathbf{k}'} = E^{\lambda} A^{\lambda}_{vc\mathbf{k}}. \tag{2.64}$$

The eigenvalues of this Hamiltonian are interpreted as exciton energies, and the eigenvectors as the corresponding wavefunctions. With them we can express L as

$$L_{v_1c_1\mathbf{k}_1,v_2c_2\mathbf{k}_2}(\omega) = -2i\sum_{\lambda} \frac{A^{\lambda}_{v_1c_1\mathbf{k}_1}\left[A^{\lambda}_{v_2c_2\mathbf{k}_2}\right]^*}{E^{\lambda} - \omega}$$

Optical Properties from the BSE

One can define the macroscopic dielectric function $\epsilon_M(\mathbf{q},\omega)$ as

$$\varepsilon_M(\mathbf{q},\omega) = \left[\varepsilon_{00}^{-1}(\mathbf{q},\omega)\right]^{-1}. \tag{2.65}$$

The optical absorption spectrum is then defined as the imaginary part of the macroscopic dielectric function in the limit $\mathbf{q} \to 0$. By introducing a new polarizability $\bar{P}$, which neglects the long-wavelength contribution of the Coulomb potential, we define the short wavlength part of the Coulomb potential as

$$\bar{v}(\mathbf{q}+\mathbf{G}) = \begin{cases} 0 & \text{for } \mathbf{G} = \mathbf{0} \\ v(\mathbf{q}+\mathbf{G}) & \text{for } \mathbf{G} \neq \mathbf{0} \end{cases}. \tag{2.66}$$

We can calculate $\bar{L}$ with the BSE by replacing $\bar{v} \to v$ in the interaction kernel Ξ. $\bar{P}$ is then obtained by making use of Eq. 2.47. It can be shown that the macroscopic dielectric function becomes

$$\varepsilon_M(\mathbf{q},\omega) = 1 - v(\mathbf{q})\bar{P}_{00}(\mathbf{q},\omega). \tag{2.67}$$

The absorption spectrum is obtained by solving the BSE for $\bar{L}$, then transforming $\bar{L}$ back to real space and calculating the matrix element $\bar{P}_{00}$. After a few further manipulations, we arrive at the final form of the absorption spectrum

$$\operatorname{Im}\varepsilon_M(\mathbf{q}\to\mathbf{0},\omega) = \frac{8\pi^2}{\Omega}\sum_{\lambda}\left|\sum_{vc\mathbf{k}} A^{\lambda}_{vc\mathbf{k}}\frac{\langle v\mathbf{k}|\,\hat{\mathbf{p}}\,|c\mathbf{k}\rangle}{\epsilon_{c\mathbf{k}}-\epsilon_{v\mathbf{k}}}\right|^2 \delta(E^{\lambda}-\omega), \tag{2.68}$$

where $\langle v\mathbf{k}|\,\hat{\mathbf{p}}\,|c\mathbf{k}\rangle$ are the transition matrix elements of the momentum operator and Ω is the unit cell volume of the crystal.

3 Many-Body Perturbation Theory in exciting

3.1 The G_0W_0 Equations in Matrix Form

Here, we explain how the G_0W_0 equations can be evaluated efficiently within the exciting code [7]. In order to do so, we need an appropriate basis to expand the desired expressions. From Eq. 2.30 it is evident that we are interested in the quantities

$$\begin{aligned}\Sigma^x_{n\mathbf{k}} &\equiv \int_V \mathrm{d}\mathbf{r} \int_V \mathrm{d}\mathbf{r}' \left[\psi_{n\mathbf{k}}(\mathbf{r})\right]^* \Sigma^x\left(\mathbf{r},\mathbf{r}'\right) \psi_{n\mathbf{k}}\left(\mathbf{r}'\right) \\ &= -\sum_{m\mathbf{k}'} f_{m\mathbf{k}'} \int_V \mathrm{d}\mathbf{r} \int_V \mathrm{d}\mathbf{r}' \left[\psi_{n\mathbf{k}}(\mathbf{r})\right]^* \psi_{m\mathbf{k}'}(\mathbf{r}) v\left(\mathbf{r},\mathbf{r}'\right) \psi_{n\mathbf{k}}\left(\mathbf{r}'\right) \left[\psi_{m\mathbf{k}'}(\mathbf{r}')\right]^* \end{aligned} \tag{3.1}$$

and

$$\begin{aligned}\Sigma^c_{n\mathbf{k}}(\omega) &\equiv \int_V \mathrm{d}\mathbf{r} \int_V \mathrm{d}\mathbf{r}' \left[\psi_{n\mathbf{k}}(\mathbf{r})\right]^* \Sigma^c\left(\mathbf{r},\mathbf{r}';\omega\right) \psi_{n\mathbf{k}}\left(\mathbf{r}'\right) \\ &= \sum_{m\mathbf{k}'} \int \mathrm{d}\mathbf{r} \int \mathrm{d}\mathbf{r}' \qquad (3.2) \\ &\quad \frac{i}{2\pi} \int \mathrm{d}\omega' \frac{1}{\omega+\omega'-\tilde{\epsilon}_{m\mathbf{k}'}} \left[\psi_{n\mathbf{k}}(\mathbf{r})\right]^* \psi_{m\mathbf{k}'}(\mathbf{r}) W_0^c\left(\mathbf{r},\mathbf{r}';\omega'\right) \psi_{n\mathbf{k}}\left(\mathbf{r}'\right) \left[\psi_{m\mathbf{k}'}\left(\mathbf{r}'\right)\right]^* . \qquad (3.3)\end{aligned}$$

Here, the integrals extend over the whole crystal space $V = N_c\Omega$. We see that in both expressions products of two Kohn-Sham functions appear. This motivates the introduction of a basis that is appropriate to describe these products. Hence, we introduce basis functions $\chi_i^{\mathfrak{q}}(\mathbf{r})$, that are normalized within in the unit cell volume Ω. Then we can

write

$$\psi_{n\mathbf{k}}(\mathbf{r})\psi^*_{m\mathbf{k}-\mathbf{q}}(\mathbf{r}) = \sum_i M^i_{nm}(\mathbf{k},\mathbf{q})\chi^{\mathbf{q}}_i(\mathbf{r}) \tag{3.4}$$

with $M^i_{nm}(\mathbf{k},\mathbf{q})$ being expansion coefficients, which can be calculated to be

$$M^i_{nm}(\mathbf{k},\mathbf{q}) \equiv \int_\Omega \left[\chi^{\mathbf{q}}_i(\mathbf{r})\psi_{m\mathbf{k}-\mathbf{q}}(\mathbf{r})\right]^* \psi_{n\mathbf{k}}(\mathbf{r})\mathrm{d}\mathbf{r}. \tag{3.5}$$

This basis is referred to as product basis and its explicit construction can be seen in Ref. [7]. The next step is to expand the bare Coulomb potential, as well as the screened Coulomb potential in this basis. One writes

$$v\left(\mathbf{r},\mathbf{r}'\right) = \sum_{\mathbf{q}}^{\mathrm{BZ}} \sum_{i,j} v_{ij}(\mathbf{q})\chi^{\mathbf{q}}_i(\mathbf{r}) \left[\chi^{\mathbf{q}}_j\left(\mathbf{r}'\right)\right]^* \tag{3.6}$$

$$W^c\left(\mathbf{r},\mathbf{r}',\omega\right) = \sum_{\mathbf{q}}^{\mathrm{BZ}} \sum_{i,j} W^c_{ij}(\mathbf{q},\omega)\chi^{\mathbf{q}}_i(\mathbf{r}) \left[\chi^{\mathbf{q}}_j\left(\mathbf{r}'\right)\right]^*, \tag{3.7}$$

and inserts the bare Coulomb potential into Eq. 3.1, to arrive at the expression for the exchange part

$$\Sigma^x_{n\mathbf{k}} = -\frac{1}{N_c}\sum_{\mathbf{q}}^{BZ}\sum_{i,j} v_{ij}(\mathbf{q}) \sum_m f_{m\mathbf{k}-\mathbf{q}} \left[M^i_{nm}(\mathbf{k},\mathbf{q})\right]^* M^j_{nm}(\mathbf{k},\mathbf{q}). \tag{3.8}$$

Here, we see that the Coulomb potential appears together with the expansion coefficients $M^i_{nm}(\mathbf{k},\mathbf{q})$. Therefore, it is numerically convenient to introduce a symmetrized form of the Coulomb potential, which can be split up to the expansion coefficients by writing

$$\tilde{M}^i_{nm}(\mathbf{k},\mathbf{q}) \equiv \sum_j \sqrt{v_{ij}(\mathbf{q})} M^j_{nm}(\mathbf{k},\mathbf{q}). \tag{3.9}$$

In this way the exchange part of the self-energy can be written as

$$\Sigma^x_{n\mathbf{k}} = -\frac{1}{N_c}\sum_{\mathbf{q}}^{BZ}\sum_{i,j}\sum_m f_{m\mathbf{k}-\mathbf{q}} \left[\tilde{M}^i_{nm}(\mathbf{k},\mathbf{q})\right]^* \tilde{M}^j_{nm}(\mathbf{k},\mathbf{q}). \tag{3.10}$$

By inserting the matrix representation of W_{ij}^c in Eq. 3.2, we find following result

$$\Sigma_{n\mathbf{k}}^c(\omega) = \frac{1}{N_c}\sum_{\mathbf{q}}^{BZ}\sum_m \frac{i}{2\pi}\int_{-\infty}^{\infty} \mathrm{d}\omega' \frac{X_{nm}\left(\mathbf{k},\mathbf{q};\omega'\right)}{\omega+\omega'-\tilde{\epsilon}_{m\mathbf{k}-\mathbf{q}}}, \tag{3.11}$$

where we introduced the abbreviation

$$X_{nm}(\mathbf{k},\mathbf{q};\omega) \equiv \sum_{ij}\left[M_{nm}^i(\mathbf{k},\mathbf{q})\right]^* W_{ij}^c(\mathbf{q},\omega) M_{nm}^j(\mathbf{k},\mathbf{q}). \tag{3.12}$$

Now we discuss how to obtain the matrix elements of the screened interaction W_{ij}^c. The polarizability is defined in Eq. 2.39, and we can conveniently calculate its matrix elements as

$$\begin{aligned}\hat{P}_{ij}^0(\mathbf{q},\omega) &\equiv \int_V\int_V \left[\chi_i^{\mathbf{q}}(\mathbf{r})\right]^* \hat{P}_0\left(\mathbf{r},\mathbf{r}';\omega\right)\chi_j^{\mathbf{q}}\left(\mathbf{r}'\right)\mathrm{d}\mathbf{r}\mathrm{d}\mathbf{r}' \\ &= \frac{1}{N_c}\sum_{\mathbf{k}}^{BZ}\sum_{n,m} F_{nm}(\mathbf{k},\mathbf{q};\omega) M_{nm}^i(\mathbf{k},\mathbf{q})\left[M_{nm}^j(\mathbf{k},\mathbf{q})\right]^*.\end{aligned} \tag{3.13}$$

For the dielectric function, we use a symmetrized form with respect to the Coulomb potential. This allows us to use the modified matrix elements from Eq. 3.9 again. We obtain following expression

$$\begin{aligned}\varepsilon_{ij}(\mathbf{q},\omega) &= \delta_{ij} - \sum_{lm}\sqrt{v_{il}(\mathbf{q})}\hat{P}_{lm}^0(\mathbf{q},\omega)\sqrt{v_{mj}(\mathbf{q})} \\ &= \delta_{ij} - \frac{1}{N_c}\sum_{\mathbf{k}}^{BZ}\sum_{n,m} F_{nm}(\mathbf{k},\mathbf{q};\omega)\tilde{M}_{nm}^i(\mathbf{k},\mathbf{q})\left[\tilde{M}_{nm}^j(\mathbf{k},\mathbf{q})\right]^*.\end{aligned} \tag{3.14}$$

After inverting the dielectric function, we can calculate the matrix elements of the correlation part of the screened interaction

$$W_{ij}^c(\mathbf{q},\omega) = \sum_{lm}\sqrt{v_{il}(\mathbf{q})}\left[\varepsilon_{lm}^{-1}(\mathbf{q},\omega)-\delta_{lm}\right]\sqrt{v_{mj}(\mathbf{q})}. \tag{3.15}$$

If we insert this in Eq. 3.12, we arrive at following expression for the auxiliary quantity X_{nm}

$$X_{nm}(\mathbf{k},\mathbf{q};\omega) \equiv \sum_{ij} \left[\tilde{M}^{i}_{nm}(\mathbf{k},\mathbf{q})\right]^{*} \left[\varepsilon^{-1}_{ij}(\mathbf{q},\omega) - \delta_{ij}\right] \tilde{M}^{j}_{nm}(\mathbf{k},\mathbf{q}). \tag{3.16}$$

3.1.1 Treatment of the Γ-Singularity

In reciprocal space, the Coulomb potential exhibits a divergence as $\mathbf{q}$ approaches zero, which gives rise to numerical challenges. This divergence is particularly evident in the plane wave basis, where the expression for the Coulomb potential takes the form

$$v_{\mathbf{G}\mathbf{G}'}(\mathbf{q}) = \frac{4\pi}{|\mathbf{q}+\mathbf{G}|^2}\delta_{\mathbf{G}\mathbf{G}'}. \tag{3.17}$$

From this equation, it becomes apparent that the singularity is confined to the component where $\mathbf{G} = \mathbf{G}' = \mathbf{0}$. As a result, it is common practice to isolate this particular component and handle the singularity separately. Especially, one can split up the Coulomb potential in a singular $v^{s}_{\mathbf{G}\mathbf{G}'}$ and a regular $\tilde{v}_{\mathbf{G}\mathbf{G}'}$ part, by writing

$$v_{\mathbf{G}\mathbf{G}'}(\mathbf{q}\to 0) = v^{s}_{\mathbf{G}\mathbf{G}'}\frac{1}{|\mathbf{q}|^2} + \tilde{v}_{\mathbf{G}\mathbf{G}'}, \tag{3.18}$$

with

$$v^{s}_{\mathbf{G}\mathbf{G}'} = 4\pi\delta_{\mathbf{G}\mathbf{0}}\delta_{\mathbf{0}\mathbf{G}'} \tag{3.19}$$

$$\tilde{v}_{\mathbf{G}\mathbf{G}'} = \frac{4\pi}{|\mathbf{G}|^2}\delta_{\mathbf{G}\mathbf{G}'}(1-\delta_{\mathbf{G}\mathbf{0}}). \tag{3.20}$$

However, accomplishing this task in the exciting implementation is not straightforward, since the singularity of the Coulomb potential extends beyond a single matrix element. In the subsequent discussion, we explore a basis transformation that still enables us to manage the singularity using conventional techniques, as outlined in Ref. [10].

The central concept is to introduce a new basis in which the Coulomb potential takes on a diagonal form. When $\mathbf{q} \neq \mathbf{0}$, achieving this goal is straightforward since the matrix representing the Coulomb potential does not encompass divergent elements. Consequently, one can compute the potential within the mixed product basis, perform its diagonalization, and utilize the resultant eigenvectors as the new basis vectors. However, when approaching the limit $\mathbf{q} \to \mathbf{0}$, a distinct approach becomes necessary due to the divergence of the Coulomb potential. In principle, it is again possible to isolate the

q dependence, as seen in Eq. 3.18 for the plane wave basis. Hence, within the mixed product basis, we can also express this as

$$v_{ij}(\mathbf{q} \to 0) = \frac{v^s_{ij}}{|\mathbf{q}|^2} + \tilde{v}_{ij}, \tag{3.21}$$

although it's important to note that the singular component is no longer confined to a single element. The regular part can be evaluated in the mixed product basis due to its absence of divergencies. Subsequently it is diagonalized and its eigenvectors are used to construct the basis. In this way, the contribution of the singular part is still missing. We know that it should be the same as in the plane wave basis, as both bases are mathematically equivalent. Therefore, we artificially set

$$v^s_{\mu\nu} = 4\pi\delta_{\mu 0}\delta_{\nu 0}, \tag{3.22}$$

where the indices $\mu\nu$ denote the new basis, in which the Coulomb potential is diagonal. As the eigenvectors explicitly only appear in expressions of the form as in Eq. 3.5, we add the $\mathbf{G} = 0$ contribution by setting

$$M^{\mu=0}_{nm}(\mathbf{k}, \mathbf{q} \to 0) = \frac{1}{\sqrt{\Omega}} M^{\mathbf{G}=0}_{nm}(\mathbf{k}, \mathbf{q} \to 0), \tag{3.23}$$

where $M^{\mathbf{G}}_{nm}(\mathbf{k}, \mathbf{q})$ will be defined in Eq. 3.45. Overall, we constructed a basis in which the diverging component of the Coulomb potential is set to the one of the plane wave basis and where the other eigenvalues are finite. In this way we can apply standard techniques to address the singularity in the following.

We need to address the singularity in three distinct equations in the *GW* implementation:

1. The exchange part of the self-energy
2. The correlation part of the self-energy
3. The dielectric function

The expressions for exchange part in Eq. 3.1 and correlation part in Eq. 3.2 contain both a sum over the vectors of the first Brillouin zone. One usually replaces the $\mathbf{q} = \mathbf{0}$ term in the sum by an average over a small region Ω_0. We abbreviate the terms under the sum with $S^{x/c}_{n\mathbf{k}}(\mathbf{q})$ and write

$$\Sigma^{x/c}_{n\mathbf{k}} = \sum_{\mathbf{q}}^{BZ} S^{x/c}_{n\mathbf{k}}(\mathbf{q}) = \sum_{\mathbf{q}\neq\mathbf{0}}^{BZ} S^{x/c}_{n\mathbf{k}}(\mathbf{q}) + \frac{1}{\Omega_0}\int_{\Omega_0} \mathrm{d}\mathbf{q} S^{x/c}_{n\mathbf{k}}(\mathbf{q}). \tag{3.24}$$

Here, the small region Ω_0 around $\mathbf{q} = 0$ is typically defined as the volume that one $\mathbf{q}$ point occupies in the Brillouin zone

$$\Omega_0 = \frac{\Omega_{BZ}}{N_q}. \tag{3.25}$$

After transforming the function S^x to the Coulomb diagonal basis, we find the following expression

$$S^x_{n\mathbf{k}}(\mathbf{q}) = -\frac{1}{N_c}\sum_{\mu} v_\mu(\mathbf{q}) \sum_m f_{m\mathbf{k}-\mathbf{q}} \left[M^\mu_{nm}(\mathbf{k},\mathbf{q})\right]^* M^\mu_{nm}(\mathbf{k},\mathbf{q}). \tag{3.26}$$

In the limit $\mathbf{q} \to 0$, we assume that the elements $M^\mu_{nm}(\mathbf{k},\mathbf{q})$ and the non-diverging eigenvalues of the Coulomb potential $v_\mu(\mathbf{q})$ to be constant when compared to the $v_0(\mathbf{q})$ element. Furthermore, we can insert $\mathbf{q} = \mathbf{0}$ in Eq. 3.23 and find

$$M^{\mu=0}_{nm}(\mathbf{k},0) = \frac{1}{\sqrt{\Omega}}\delta_{nm}, \tag{3.27}$$

which we insert for the $\mu = 0$ contribution. Overall, we arrive at following expression for the integral of S^x

$$\begin{aligned}\int S^x_{n\mathbf{k}}(\mathbf{q})\mathrm{d}\mathbf{q} = &-\frac{1}{N_c}\sum_{\mu\neq 0} v_\mu(0)\sum_m f_{m\mathbf{k}}\left[M^\mu_{nm}(\mathbf{k},0)\right]^* M^\mu_{nm}(\mathbf{k},0) \\ &-\frac{f_{n\mathbf{k}}}{V}\int_{\Omega_0} v_0(\mathbf{q})\mathrm{d}\mathbf{q}.\end{aligned} \tag{3.28}$$

In order to calculate the integral of the diverging element of the Coulomb potential, the so-called spherical approximation is made, where Ω_0 is assumed to be a sphere. In this case, one can easily derive a closed expression for the average of the bare Coulomb potential

$$\int_{\Omega_0} v_0(\mathbf{q})\mathrm{d}\mathbf{q} = 16\pi^2\left(\frac{3\Omega_0}{4\pi}\right)^{\frac{1}{3}}. \tag{3.29}$$

We continue to discuss the singularity in the correlation part of the self-energy. The function $S^c_{n\mathbf{k}}$ reads

$$S^c_{n\mathbf{k}}(\mathbf{q},\omega) = \frac{1}{N_c}\sum_m \frac{i}{2\pi}\int_{-\infty}^{\infty} \mathrm{d}\omega' \frac{X_{nm}\left(\mathbf{k},\mathbf{q};\omega'\right)}{\omega+\omega'-\tilde{\epsilon}_{m\mathbf{k}-\mathbf{q}}}. \tag{3.30}$$

By assuming the eigenvalues $\tilde{\epsilon}_{m\mathbf{k}-\mathbf{q}}$ are not strongly $\mathbf{q}$ dependent, the quantity that needs to be averaged is X_{nm}, which reads in the Coulomb diagonal basis

$$X_{nm}(\mathbf{k},\mathbf{q};\omega) \equiv \sum_{\mu\nu} \left[M^\mu_{nm}(\mathbf{k},\mathbf{q})\right]^* W^c_{\mu\nu}(\mathbf{q},\omega) M^\nu_{nm}(\mathbf{k},\mathbf{q}). \tag{3.31}$$

If we further assume that the only relevant $\mathbf{q}$ dependence lies within the matrix elements $W^c_{\mu\nu}$, we can write the average as

$$\begin{aligned}\int_{\Omega_0} X_{nm}(\mathbf{k},\mathbf{q};\omega)\mathrm{d}\mathbf{q} = &\sum_{\mu\nu\neq 0}\left[M^\mu_{nm}(\mathbf{k},\mathbf{0})\right]^* \int_{\Omega_0} W^c_{\mu\nu}(\mathbf{q},\omega)\mathrm{d}\mathbf{q} M^\nu_{nm}(\mathbf{k},\mathbf{0}) \\ &+ \frac{\delta_{nm}}{\Omega}\int_{\Omega_0} W^c_{00}(\mathbf{q},\omega)\mathrm{d}\mathbf{q} \\ &+ \frac{\delta_{nm}}{\sqrt{\Omega}}\sum_{\mu\neq 0}\int_{\Omega_0} W^c_{0\mu}(\mathbf{q},\omega)\mathrm{d}\mathbf{q} M^\mu_{nm}(\mathbf{k},\mathbf{0}) \\ &+ \frac{\delta_{nm}}{\sqrt{\Omega}}\sum_{\mu\neq 0}\int_{\Omega_0} W^c_{\mu 0}(\mathbf{q},\omega)\mathrm{d}\mathbf{q}\left[M^\mu_{nm}(\mathbf{k},\mathbf{0})\right]^*. \end{aligned} \tag{3.32}$$

The remaining task is, to perform the integration over the matrix elements of the screened Coulomb potential. However, it is not as straightforward as for the bare Coulomb potential, as the inverse dielectric function also appears under the integral. Thus, we now explore the $\mathbf{q}$ dependence of the matrix elements of the dielectric function in the long-wavelength limit. It is expected that only the head ε_{00} and the wings $\varepsilon_{\mu 0}$ and $\varepsilon_{0\mu}$ may contain potential divergences arising from the Coulomb interaction. From Eq. 3.14, it is evident that the dielectric function relies on the polarizability of the system. To investigate its $\mathbf{q}$ dependence, we apply an approximation [11] for the M^0_{nm} elements

$$M^0_{nm}(\mathbf{k},\mathbf{q}\to\mathbf{0}) = \frac{1}{\sqrt{\Omega}}\frac{\mathbf{q}\cdot\mathbf{p}_{nm,\mathbf{k}}}{\epsilon_{m\mathbf{k}}-\epsilon_{n\mathbf{k}}}, \tag{3.33}$$

where the $\mathbf{p}_{nm,\mathbf{k}}$ are matrix elements of the momentum operator

$$\mathbf{p}_{nm,\mathbf{k}} \equiv \langle n\mathbf{k}| \hat{\mathbf{p}} |m\mathbf{k}\rangle . \tag{3.34}$$

By inserting this into Eq. 3.13 we can write the head and the wings of the polarizability as

$$P_{00}(\mathbf{q} \to \mathbf{0}, \omega) = \mathbf{q} \cdot \mathcal{P}(\omega)\mathbf{q} = |\mathbf{q}|^2 \hat{\mathbf{q}} \cdot \mathcal{P}(\omega)\hat{\mathbf{q}}, \tag{3.35}$$

$$P_{\mu 0}(\mathbf{q} \to \mathbf{0}, \omega) = \mathbf{q} \cdot \mathbf{p}_\mu(\omega) = |\mathbf{q}| \hat{\mathbf{q}} \cdot \mathbf{p}_\mu(\omega), \tag{3.36}$$

$$P_{0\mu}(\mathbf{q} \to \mathbf{0}, \omega) = \mathbf{q} \cdot \mathbf{s}_\mu(\omega) = |\mathbf{q}| \hat{\mathbf{q}} \cdot \mathbf{s}_\mu(\omega), \tag{3.37}$$

with a 3×3-tensor $\mathcal{P}$ and the vectors $\mathbf{p}_\mu$ and $\mathbf{s}_\mu$ which are defined as

$$\mathbf{p}_\mu(\omega) = \frac{1}{N_c\sqrt{\Omega}} \sum_{n,m} \sum_{\mathbf{k}} F_{nm}(\mathbf{k}, \mathbf{0}; \omega) \frac{\mathbf{p}_{nm,\mathbf{k}}}{\epsilon_{m\mathbf{k}} - \epsilon_{n\mathbf{k}}} \left[M^\mu_{nm}(\mathbf{k}, \mathbf{0})\right]^* \tag{3.38}$$

$$\mathbf{s}_\mu(\omega) = \frac{1}{N_c\sqrt{\Omega}} \sum_{n,m} \sum_{\mathbf{k}} F_{nm}(\mathbf{k}, \mathbf{0}; \omega) \frac{\mathbf{p}_{nm,\mathbf{k}}}{\epsilon_{m\mathbf{k}} - \epsilon_{n\mathbf{k}}} M^\mu_{nm}(\mathbf{k}, \mathbf{0}) \tag{3.39}$$

$$\mathcal{P}(\omega) = \frac{1}{N_c\Omega} \sum_{n,m} \sum_{\mathbf{k}} F_{nm}(\mathbf{k}, \mathbf{0}; \omega) \frac{\mathbf{p}_{nm,\mathbf{k}} \otimes \mathbf{p}_{nm,\mathbf{k}}}{(\epsilon_{m\mathbf{k}} - \epsilon_{n\mathbf{k}})^2}. \tag{3.40}$$

Using this approximation for the polarizability, we arrive at the following expressions for the dielectric function

$$\varepsilon_{00}(\mathbf{q} \to \mathbf{0}, \omega) = 1 - 4\pi \hat{\mathbf{q}} \cdot \mathcal{P}(\omega)\hat{\mathbf{q}} \tag{3.41}$$

$$\varepsilon_{\mu 0}(\mathbf{q} \to \mathbf{0}, \omega) = -\sqrt{v_\mu(\mathbf{0})}\sqrt{4\pi} \hat{\mathbf{q}} \cdot \mathbf{p}_\mu(\omega) \tag{3.42}$$

$$\varepsilon_{0\mu}(\mathbf{q} \to \mathbf{0}, \omega) = -\sqrt{v_\mu(\mathbf{0})}\sqrt{4\pi} \hat{\mathbf{q}} \cdot \mathbf{s}_\mu(\omega). \tag{3.43}$$

where $\hat{\mathbf{q}}$ is the direction in which the limit is taken. The fact that the limit depends on the direction in which it is taken, is often referred to as dielctric anisotropicity [10]. For us it is also particularly useful that it is not dependent on the absolute value of $\mathbf{q}$. Hence, we can still apply the spherical approximation for averaging the screened interaction and split up the integration in a radial and angular part. The $\mu = 0$ component of the bare Coulomb potential is then averaged over the radial part as in Eq. 3.29, while the dielectric function is averaged over the angular part. It is worth noting, that due to

the matrix inversion all elements of $\varepsilon^{-1}_{\mu\nu}$ are dependent on the direction $\hat{\mathbf{q}}$, and therefore have to be averaged. The angular integration of the inverse dielectric function must be solved numerically, which is not discussed in detail here.

3.2 The BSE in Matrix Form

The implementation of the BSE in exciting uses a plane wave basis [12] to expand the relevant equations. We are interested in integrals of the type

$$\int_\Omega \psi^*_{n\mathbf{k}}(\mathbf{r}) e^{-i(\mathbf{q}+\mathbf{G})} \psi_{m\mathbf{k}'}(\mathbf{r}) \mathrm{d}\mathbf{r}. \tag{3.44}$$

It can be shown that it vanishes if $\mathbf{k}' \neq \mathbf{k}+\mathbf{q}$ [9]. Hence, we are only interested in the expansion coefficients where $\mathbf{k}' = \mathbf{k}+\mathbf{q}$ and define

$$M^{\mathbf{G}}_{nm}(\mathbf{k},\mathbf{q}) \equiv \int_\Omega \psi^*_{n\mathbf{k}}(\mathbf{r}) e^{-i(\mathbf{q}+\mathbf{G})\mathbf{r}} \psi_{m\mathbf{k}+\mathbf{q}}(\mathbf{r}) \mathrm{d}\mathbf{r}. \tag{3.45}$$

The Coulomb potential in this basis is diagonal, and has the following form

$$v_{\mathbf{G}\mathbf{G}'} = \frac{4\pi}{|\mathbf{q}+\mathbf{G}|^2} \delta_{\mathbf{G}\mathbf{G}'}. \tag{3.46}$$

For the exchange part of the BSE Hamiltonian, we use the short wave-length part defined in Eq. 2.66. Its real-space representation can be written as

$$\bar{v}\left(\mathbf{r},\mathbf{r}'\right) = \sum_{\mathbf{G}\neq\mathbf{0}} \sum_{\mathbf{q}} \frac{1}{\Omega} \frac{4\pi}{|\mathbf{q}+\mathbf{G}|} e^{-i(\mathbf{q}+\mathbf{G})(\mathbf{r}-\mathbf{r}')}. \tag{3.47}$$

By inserting it into Eq. 2.62, we arrive at

$$\begin{aligned} H^{\mathrm{x}}_{v_1c_1\mathbf{k}_1,v_2c_2\mathbf{k}_2} &= 2\sum_{\mathbf{G}\neq\mathbf{0}} \sum_{\mathbf{q}} \frac{1}{V} \int \mathrm{d}\mathbf{r}_1 \psi_{v_1\mathbf{k}_1}\left(\mathbf{r}_1\right) e^{-i(\mathbf{q}+\mathbf{G})\mathbf{r}_1} \psi^*_{c_1\mathbf{k}_1}\left(\mathbf{r}_1\right) \int \mathrm{d}\mathbf{r}_2 \psi^*_{v_2\mathbf{k}_2}\left(\mathbf{r}_2\right) e^{i(\mathbf{q}+\mathbf{G})\mathbf{r}_2} \psi_{c_2\mathbf{k}_2}\left(\mathbf{r}_2\right) \\ &= \frac{8\pi}{V} \sum_{\mathbf{G}\neq\mathbf{0}} \frac{1}{|\mathbf{G}|^2} M^{\mathbf{G}}_{v_2c_2}\left(\mathbf{k}_2,\mathbf{q}=\mathbf{0}\right) \left[M^{\mathbf{G}}_{v_1c_1}(\mathbf{k}_1,\mathbf{q}=\mathbf{0})\right]^*. \end{aligned} \tag{3.48}$$

Here, we made use of the fact, that the integrals are only non-vanishing when $\mathbf{q}=\mathbf{0}$. Therefore, the sum over the $\mathbf{q}$ vectors vanishes.

In order to evaluate the direct term of the BSE Hamiltonian, we first construct the

matrix elements of the dielectric function

$$\varepsilon_{\mathbf{G}\mathbf{G}'}(\mathbf{q},\omega) = \delta_{\mathbf{G}\mathbf{G}'} - \frac{1}{V} v_{\mathbf{G}'}(\mathbf{q}) \sum_{nm\mathbf{k}} F_{nm}(\mathbf{k},\mathbf{q};\omega) \left[M^{\mathbf{G}}_{nm}(\mathbf{k},\mathbf{q})\right]^* M^{\mathbf{G}'}_{nm}(\mathbf{k},\mathbf{q}). \tag{3.49}$$

This expression is very similar to the dielectric function in the product basis of the *GW* implementation in Eq. 3.14. The only difference is, that here one normalizes the polarizability with $1/V$, because the plane wave appearing in Eq. 3.45 is not normalized. After inverting the dielectric function, the screened interaction reads

$$W_{\mathbf{G}\mathbf{G}'}(\mathbf{q}) = \sqrt{v_{\mathbf{G}}(\mathbf{q})}\varepsilon^{-1}_{\mathbf{G}\mathbf{G}'}(\mathbf{q},\omega=0)\sqrt{v_{\mathbf{G}'}(\mathbf{q})}, \tag{3.50}$$

and its real space representation is

$$W(\mathbf{r}_1,\mathbf{r}_2) = \frac{1}{V}\sum_{\mathbf{q}}\sum_{\mathbf{G}\mathbf{G}'} e^{-i(\mathbf{q}+\mathbf{G})\mathbf{r}_1} \frac{4\pi\varepsilon^{-1}_{\mathbf{G}\mathbf{G}'}(\mathbf{q})}{|\mathbf{q}+\mathbf{G}||\mathbf{q}+\mathbf{G}'|} e^{i(\mathbf{q}+\mathbf{G}')\mathbf{r}_2}. \tag{3.51}$$

After inserting in Eq. 2.63, we find the following expression for the direct term of the BSE Hamiltonian

$$H^{\text{dir}}_{v_1c_1\mathbf{k}_1,v_2c_2\mathbf{k}_2} = -\frac{1}{V}\sum_{\mathbf{G}\mathbf{G}'} W_{\mathbf{G}\mathbf{G}'}(\mathbf{k}_2-\mathbf{k}_1)\, M^{\mathbf{G}}_{c_1c_2}(\mathbf{k},\mathbf{k}_2-\mathbf{k}_1)\left[M^{\mathrm{G}'}_{v_1v_2}(\mathbf{k},\mathbf{k}_2-\mathbf{k}_1)\right]^*. \tag{3.52}$$

Here, also the sum over the $\mathbf{q}$ vectors has disappeared, because integrals of the type as in Eq. 3.44 are non-vanishing only for $\mathbf{q} = \mathbf{k}_2 - \mathbf{k}_1$.

3.2.1 Treatment of the Γ-Singularity

The singularity of the Coulomb potential also needs to be addressed in the implementation of the BSE. However, here the treatment becomes simpler compared to the *GW* implementation. This is due to the fact that the non-local operators are expressed in terms of plane waves. Moreover, the singularity only enters in the expression of the direct Hamiltonian, Eq. 3.52. Here, we have to average the screened interaction again, for which the procedure is the same as in the *GW* part. Here, we give a brief overview

of the differences in the formulas. The polarizability can be expanded as

$$P_{\mathbf{00}}(\mathbf{q}\to\mathbf{0}) = \mathbf{q}\cdot\mathcal{P}\mathbf{q} = |\mathbf{q}|^2\hat{\mathbf{q}}\cdot\mathcal{P}\hat{\mathbf{q}}, \tag{3.53}$$

$$P_{\mathbf{G0}}(\mathbf{q}\to\mathbf{0}) = \mathbf{q}\cdot\mathbf{p}_{\mathbf{G}} = |\mathbf{q}|\hat{\mathbf{q}}\cdot\mathbf{p}_{\mathbf{G}}, \tag{3.54}$$

$$P_{\mathbf{0G}}(\mathbf{q}\to\mathbf{0}) = \mathbf{q}\cdot\mathbf{s}_{\mathbf{G}} = |\mathbf{q}|\hat{\mathbf{q}}\cdot\mathbf{s}_{\mathbf{G}}, \tag{3.55}$$

with the quantities

$$\mathbf{p}_{\mathbf{G}}(\omega) = \frac{1}{V}\sum_{n,m}\sum_{\mathbf{k}} F_{nm}(\mathbf{k},0;\omega)\frac{\mathbf{p}_{nm,\mathbf{k}}}{\epsilon_{m\mathbf{k}}-\epsilon_{n\mathbf{k}}}\left[M^{\mathbf{G}}_{nm}(\mathbf{k},0)\right]^* \tag{3.56}$$

$$\mathbf{s}_{\mathbf{G}}(\omega) = \frac{1}{V}\sum_{n,m}\sum_{\mathbf{k}} F_{nm}(\mathbf{k},0;\omega)\frac{\mathbf{p}_{nm,\mathbf{k}}}{\epsilon_{m\mathbf{k}}-\epsilon_{n\mathbf{k}}}M^{\mathbf{G}}_{nm}(\mathbf{k},0) \tag{3.57}$$

$$\mathcal{P}(\omega) = \frac{1}{V}\sum_{n,m}\sum_{\mathbf{k}} F_{nm}(\mathbf{k},0;\omega)\frac{\mathbf{p}_{nm,\mathbf{k}}\otimes\mathbf{p}_{nm,\mathbf{k}}}{(\epsilon_{m\mathbf{k}}-\epsilon_{n\mathbf{k}})^2}. \tag{3.58}$$

In this way, we can rewrite the dielectric function in the plane wave basis as

$$\varepsilon_{\mathbf{00}}(\mathbf{q}\to\mathbf{0},\omega) = 1 - 4\pi\hat{\mathbf{q}}\cdot\mathcal{P}(\omega)\hat{\mathbf{q}} \tag{3.59}$$

$$\varepsilon_{\mathbf{G0}}(\mathbf{q}\to\mathbf{0},\omega) = -\sqrt{v_{\mathbf{G}}(\mathbf{0})}\sqrt{4\pi}\hat{\mathbf{q}}\cdot\mathbf{p}_{\mathbf{G}}(\omega) \tag{3.60}$$

$$\varepsilon_{\mathbf{0G}}(\mathbf{q}\to\mathbf{0},\omega) = -\sqrt{v_{\mathbf{G}}(\mathbf{0})}\sqrt{4\pi}\hat{\mathbf{q}}\cdot\mathbf{s}_{\mathbf{G}}(\omega). \tag{3.61}$$

The averaging of the screened interaction can be performed in the same way as in the GW implementation.

4 Coulomb Cutoffs for Low-Dimensional Materials

Simulating low-dimensional materials in computer codes with 3D periodic boundary conditions, such as `exciting`, requires the incorporation of vacuum to mimic the reduced dimensionality. The inclusion of vacuum allows for the separation and isolation of individual layers, nanowires, or molecules within the computational framework. However, in practice it can be difficult to include a sufficient amount of vacuum to completely turn off the interaction between periodically repeated images. Therefore, a scheme was proposed in Ref. [2], that cuts off the Coulomb potential between the images. The different geometries of low-dimensional materials and the resulting cutoffs are discussed in this chapter following Ref. [2].

4.1 2D Materials

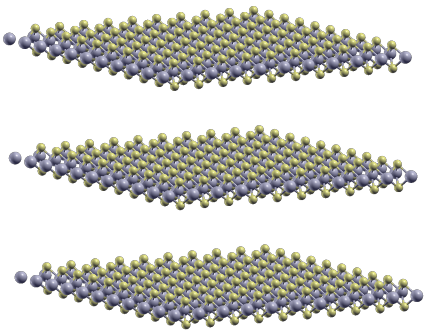

Figure 4.1: Example of slab geometry for the case of MoS_2.

We begin with the slab geometry, where the system is periodic in the xy plane. The slab is then repeated periodically along the z-direction, see Fig. 4.1. In order to cut off the interaction between the layers, we choose a truncation length r_c and define the modified

Coulomb potential as follows

$$v(\mathbf{r}_\parallel, z) = \frac{\theta(r_c - |z|)}{\sqrt{|\mathbf{r}_\parallel|^2 + z^2}}. \tag{4.1}$$

Here, θ denotes the Heaviside step function and $\mathbf{r}_\parallel$ is the coordinate in the xy plane. The Fourier transform of the truncated Coulomb potential can then be calculated to be

$$v^{\mathrm{2D}}(\mathbf{k}) = \frac{4\pi}{|\mathbf{k}|^2}\left\{1 + e^{-|\mathbf{k}_\parallel| r_c}\left[\frac{k_z}{|\mathbf{k}_\parallel|}\sin(k_z r_c) - \cos(k_z r_c)\right]\right\}, \tag{4.2}$$

where $|\mathbf{k}_\parallel| = \sqrt{k_x^2 + k_y^2}$. Notably, this formula diverges when $|\mathbf{k}_\parallel| \to 0$ for any nonzero k_z and is unsuitable for arbitrary r_c. However, this problem can be solved by choosing $r_c = L_z/2$, where L_z is the distance between the layers. In this case, the $\sin(k_z r_c)$ term vanishes, since the reciprocal lattice vectors can be written as $k_z = 2\pi n_z/L_z$ for integer n_z, leading to $k_z r_c = \pi n_z$. Consequently, expression simplifies to

$$\hat{v}^{\mathrm{2D}}(\mathbf{k}) = \frac{4\pi}{|\mathbf{k}|^2}\left\{1 - e^{-|\mathbf{k}_\parallel| r_c}\cos(k_z r_c)\right\}. \tag{4.3}$$

Now, the Coulomb interaction is finite for any $|\mathbf{k}_\parallel|$ when $k_z \neq 0$. For $k_z = 0$, it diverges as $4\pi r_c/|\mathbf{k}_\parallel|$ when $|\mathbf{k}_\parallel| \to 0$, which is milder than the untruncated 3D case. Thus, our choice of r_c confines the divergence to the single wave vector $k = 0$.

4.2 1D Materials

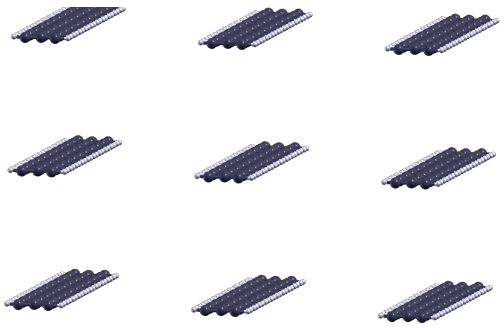

Figure 4.2: Example for a wire geometry in the case of poly(para-phenylene).

In the wire geometry, the periodic direction is usually chosen to be along the z-axis, and the system is confined in the xy plane, see Fig. 4.2. Similarly to the 2D case,

we introduce a cutoff by turning off the interaction outside a certain region. This is expressed by the function $\theta(x, y)$, which is one if x and y lie in a finite region around the wire, and zero if x and y lie outside the region. The specific choice of the region will be discussed below. In real space the 1D truncated Coulomb potential reads

$$v^{1\mathrm{D}}(\mathbf{r}) = \frac{\theta(x, y)}{|\mathbf{r}|}. \tag{4.4}$$

With this general form, we can calculate the Fourier transform in z-direction, which yields

$$v^{1\mathrm{D}}(\mathbf{k}) = \int dx \int dy\, \theta(x, y)\, 2K_0(|k_z||\mathbf{r}_\parallel|)\, \cos(k_x x + k_y y). \tag{4.5}$$

This expression contains the modified Bessel function $K_0(|k_z||\mathbf{r}_\parallel|)$. It diverges as $k_z \to 0$, and the asymptotic form can be written as

$$K_0(|k_z||\mathbf{r}_\parallel|) = -\ln\big(|k_z||\mathbf{r}_\parallel|\big) + O(z^0). \tag{4.6}$$

As the xy integral is over a finite region, the divergences in $v^{1\mathrm{D}}(\mathbf{k})$ arise due to the asymptotic behavior of K_0. Hence, the divergent term of the Coulomb potential is

$$-2\ln(|k_z|) \int dx \int dy\, \theta(x, y)\, \cos(k_x x + k_y y). \tag{4.7}$$

To eliminate this divergence for any wave vector with $k_{xy} \neq 0$, we restrict the basis vectors in the xy plane to be orthogonal and set $\theta(x, y) \neq 0$ in exactly one Wigner-Seitz cell centered on the wire in the xy plane. In this way, the x and y integration can be written as

$$\int dx \int dy\, \theta(x, y)\, \cos(k_x x + k_y y) = \frac{4\sin(k_x a/2)\sin(k_y b/2])}{k_x k_y}, \tag{4.8}$$

with a and b being the length of the lattice vectors in the xy plane. In the 1D case, k_x and k_y are reciprocal lattice vectors, turning the integral above zero. This means, that the divergence in Eq. 4.7 gets restricted to the case $k_x = k_y = k_z = 0$. The expression in Eq. 4.5 cannot be simplified further, meaning that $v^{1\mathrm{D}}(\mathbf{k})$ must be computed numerically.

4.3 0D Materials

For 0D materials, the most natural choice is to cut off the Coulomb interaction outside a sphere of radius r_c,

$$v_c^{\mathrm{0D}}(\mathbf{r}) = \theta(r_c - |\mathbf{r}|)\frac{1}{|\mathbf{r}|}. \tag{4.9}$$

This leads to a closed expression in reciprocal space

$$v_c^{\mathrm{0D}} = \frac{4\pi}{|\mathbf{k}|^2}\left(1 - \cos(|\mathbf{k}|r_c)\right). \tag{4.10}$$

This truncated interaction remains finite for any wave vector $\mathbf{k}$. However, one has to be careful with the choice of the cutoff radius r_c. In `exciting`, it is chosen to $r_c = L_z/2$, where L_z is the length of the unit cell in z-direction. With this choice it could happen that one cuts off intramolecular interactions accidentally.

4.4 Analytic Expressions of the 2D Screened Potential

In the current implementation of `exciting` the treatment of the singularity as outlined in Sec. 3.1.1 was not fully adapted to the case of an applied Coulomb cutoff and its altered $\mathbf{q}$ dependence. In the case of the GW implementation, the singular terms of the matrix of the screened interaction were set to zero. Leaving this contribution out requires a much denser sampling of $\mathbf{q}$ points to capture the behavior of the screened potential near the Γ point. Similarly, in the BSE implementation the treatment of the singularity was not adapted to the cutoff potential, completely ignoring the altered $\mathbf{q}$ dependence. Overall, this motivates the need of a more sophisticated method to treat the singularity. In Ref. [3] the following analytical expressions for the correlation part

of the screened interaction with a 2D cutoff were derived in a plane wave basis

$$W^c_{\mathbf{00}}(\mathbf{q}\to\mathbf{0}) = -\left(\frac{4\pi\left(1-e^{-|\mathbf{q}|L/2}\right)}{|\mathbf{q}|}\right)^2 \frac{\hat{\mathbf{q}}\cdot\mathbf{A}\hat{\mathbf{q}}}{1+4\pi\left(1-e^{-|\mathbf{q}|L/2}\right)\hat{\mathbf{q}}\cdot\mathbf{A}\hat{\mathbf{q}}}, \tag{4.11}$$

$$W^c_{\mathbf{G0}}(\mathbf{q}\to\mathbf{0}) = -\frac{4\pi\left(1-e^{-|\mathbf{q}|L/2}\right)}{|\mathbf{q}|}\frac{\sqrt{v_{\mathbf{G}}(\mathbf{0})}\hat{\mathbf{q}}\cdot\mathbf{a}_{\mathbf{G}}}{1+4\pi\left(1-e^{-|\mathbf{q}|L/2}\right)\hat{\mathbf{q}}\cdot\mathbf{A}\hat{\mathbf{q}}}, \tag{4.12}$$

$$W^c_{\mathbf{0G}}(\mathbf{q}\to\mathbf{0}) = -\frac{4\pi\left(1-e^{-|\mathbf{q}|L/2}\right)}{|\mathbf{q}|}\frac{\sqrt{v_{\mathbf{G}}(\mathbf{0})}\hat{\mathbf{q}}_{\parallel}\cdot\mathbf{b}_{\mathbf{G}}}{1+4\pi\left(1-e^{-|\mathbf{q}|L/2}\right)\hat{\mathbf{q}}\cdot\mathbf{A}\hat{\mathbf{q}}}, \tag{4.13}$$

$$W^c_{\mathbf{GG'}}(\mathbf{q}\to\mathbf{0}) = \sqrt{v_{\mathbf{G}}(\mathbf{0})v_{\mathbf{G'}}(\mathbf{0})}\left[B^{-1}_{\mathbf{GG'}} - \delta_{\mathbf{GG'}} + \frac{4\pi\left(1-e^{-|\mathbf{q}|L/2}\right)\left(\hat{\mathbf{q}}\cdot\mathbf{a}_{\mathbf{G}}\right)\left(\hat{\mathbf{q}}\cdot\mathbf{b}_{\mathbf{G'}}\right)}{1+4\pi\left(1-e^{-|\mathbf{q}|L/2}\right)\hat{\mathbf{q}}\cdot\mathbf{A}\hat{\mathbf{q}}}\right]. \tag{4.14}$$

Here, A is a 3×3 tensor and $\mathbf{a_G}$ and $\mathbf{b_G}$ are 3D vectors, that will be properly introduced in the next chapter in Eq. 5.11 to Eq. 5.13. It is worth noting, that the reduced dimensionality leads to non-divergent behavior of the head contribution. While it diverges in the 3D case, it now converges to the finite value

$$W^c_{\mathbf{00}}(\mathbf{q}=\mathbf{0}) = -(2\pi L)^2\hat{\mathbf{q}}\cdot\hat{\mathbf{A}}\hat{\mathbf{q}}. \tag{4.15}$$

Nevertheless, it remains beneficial to integrate the analytical expressions over a small region around $\mathbf{q}=\mathbf{0}$, in order to capture all long-wavelength contributions to the screening.

5 Efficient Screening in Low-Dimensional Materials

In this chapter, we generalize the derivation of the analytic expressions for the correlation part of the screened Coulomb potential to 1D and 0D materials. Then the implementation of these analytic expressions to `exciting` is described. We follow the derivation from Ref. [3] using an arbitrarily $\mathbf{q}$ dependent bare Coulomb potential. It is crucial to note that the main ingredients of this derivation are the long-wavelength limit of the polarizability and the diverging element of the Coulomb potential. We recall that the long-wavelength limit of the polarizability can be expanded analogously in both the plane wave basis (cf. Eq. 3.53 to Eq. 3.55) and the Coulomb diagonal basis (cf. Eq. 3.35 to Eq. 3.37). Furthermore, the diverging component of the bare Coulomb potential is identical in both bases by construction. Hence, we perform the derivation only in the plane wave basis, keeping in mind that it is completely analogous in the Coulomb diagonal basis.

By combining the Coulomb potential and the long wavelength limit of the polarizability from Eq. 3.53-Eq. 3.55 with the expression for the dielectric matrix Eq. 3.49, we can write

$$\varepsilon_{\mathbf{00}}(\mathbf{q}\to\mathbf{0}) = 1 - v_{\mathbf{0}}(\mathbf{q})\,|\mathbf{q}|^2\,\hat{\mathbf{q}}\cdot\mathcal{P}\hat{\mathbf{q}} \tag{5.1}$$

$$\varepsilon_{\mathbf{G0}}(\mathbf{q}\to\mathbf{0}) = -\sqrt{v_{\mathbf{G}}(\mathbf{0})}\sqrt{v_{\mathbf{0}}(\mathbf{q})}\,|\mathbf{q}|\,\hat{\mathbf{q}}\cdot\mathbf{p}_{\mathbf{G}} \tag{5.2}$$

$$\varepsilon_{\mathbf{0G}}(\mathbf{q}\to\mathbf{0}) = -\sqrt{v_{\mathbf{G}}(\mathbf{0})}\sqrt{v_{\mathbf{0}}(\mathbf{q})}\,|\mathbf{q}|\,\hat{\mathbf{q}}\cdot\mathbf{s}_{\mathbf{G}}. \tag{5.3}$$

Here, and in the rest of the derivation, we do not write the frequency dependence explicitly. We assume that the components of the Coulomb potential where $\mathbf{G}\neq 0$, are constant for small values of $\mathbf{q}$. In this way, only the head and wings are $\mathbf{q}$ dependent,

while the body is not. For the body, $\mathbf{G} \neq 0$ and $\mathbf{G'} \neq 0$, we introduce the notation

$$B_{\mathbf{G}\mathbf{G}'} \equiv \varepsilon_{\mathbf{G}\mathbf{G}'}\left(\mathbf{q} \to \mathbf{0}\right). \tag{5.4}$$

This motivates us to write the dielectric matrix in a block form, in order to treat the $\mathbf{q}$ dependence properly,

$$\boldsymbol{\varepsilon} = \begin{pmatrix} H & \mathbf{w}^{\top} \\ \mathbf{v} & \mathbf{B} \end{pmatrix}. \tag{5.5}$$

For a block matrix of the above shape, one can give a closed expression for the inverse matrix

$$\boldsymbol{\varepsilon}^{-1} = \begin{pmatrix} \left(H - \mathbf{w}^{\top}\mathbf{B}^{-1}\mathbf{v}\right)^{-1} & -\left(H - \mathbf{w}^{\top}\mathbf{B}^{-1}\mathbf{v}\right)^{-1}\mathbf{w}^{\top}\mathbf{B}^{-1} \\ -\mathbf{B}^{-1}\mathbf{v}\left(H - \mathbf{w}^{\top}\mathbf{B}^{-1}\mathbf{v}\right)^{-1} & \mathbf{B}^{-1} + \mathbf{B}^{-1}\mathbf{v}\left(H - \mathbf{w}^{\top}\mathbf{B}^{-1}\mathbf{v}\right)^{-1}\mathbf{w}^{\top}\mathbf{B}^{-1} \end{pmatrix}. \tag{5.6}$$

Writing the components of the inverse block matrix, we arrive at following expressions:

$$\varepsilon^{-1}_{\mathbf{0}\mathbf{0}} = \left[\varepsilon_{\mathbf{0}\mathbf{0}} - \sum_{\mathbf{G},\mathbf{G}'\neq\mathbf{0}} \varepsilon_{\mathbf{0}\mathbf{G}} B^{-1}_{\mathbf{G}\mathbf{G}'} \varepsilon_{\mathbf{G}'\mathbf{0}}\right]^{-1}, \tag{5.7}$$

$$\varepsilon^{-1}_{\mathbf{G}\mathbf{0}} = -\varepsilon^{-1}_{\mathbf{0}\mathbf{0}} \sum_{\mathbf{G}'\neq\mathbf{0}} B^{-1}_{\mathbf{G}\mathbf{G}'} \varepsilon_{\mathbf{G}'\mathbf{0}}, \tag{5.8}$$

$$\varepsilon^{-1}_{\mathbf{0}\mathbf{G}} = -\varepsilon^{-1}_{\mathbf{0}\mathbf{0}} \sum_{\mathbf{G}'\neq\mathbf{0}} \varepsilon_{\mathbf{0}\mathbf{G}'} B^{-1}_{\mathbf{G}'\mathbf{G}}, \tag{5.9}$$

$$\varepsilon^{-1}_{\mathbf{G}\mathbf{G}'} = B^{-1}_{\mathbf{G}\mathbf{G}'} + \varepsilon^{-1}_{\mathbf{0}\mathbf{0}} \left(\sum_{\mathbf{G}''\neq\mathbf{0}} B^{-1}_{\mathbf{G}\mathbf{G}''} \varepsilon_{\mathbf{G}''\mathbf{0}}\right)\left(\sum_{\mathbf{G}''\neq\mathbf{0}} \varepsilon_{\mathbf{0}\mathbf{G}''} B^{-1}_{\mathbf{G}''\mathbf{G}'}\right). \tag{5.10}$$

It can be simplified by introducing the auxiliary vectors $\mathbf{a}_{\mathbf{G}}, \mathbf{b}_{\mathbf{G}}$ and the tensor A given by

$$\mathbf{a}_{\mathbf{G}} = -\sum_{\mathbf{G}'\neq\mathbf{0}} B^{-1}_{\mathbf{G}\mathbf{G}'} \sqrt{v_{\mathbf{G}'}(\mathbf{0})} \mathbf{p}_{\mathbf{G}'}, \tag{5.11}$$

$$\mathbf{b}_{\mathbf{G}} = -\sum_{\mathbf{G}'\neq\mathbf{0}} \sqrt{v_{\mathbf{G}'}(\mathbf{0})} \mathbf{s}_{\mathbf{G}'} B^{-1}_{\mathbf{G}'\mathbf{G}}, \tag{5.12}$$

$$\mathbf{A} = -\mathcal{P} - \sum_{\mathbf{G}\neq\mathbf{0}} \sqrt{v_{\mathbf{G}}\left(\mathbf{0}\right)} \mathbf{s}_{\mathbf{G}} \otimes \mathbf{a}_{\mathbf{G}}, \tag{5.13}$$

where $\otimes$ denotes the tensor product. The simplified long wavelength limit of the inverse

dielectric function is then

$$\varepsilon^{-1}_{\mathbf{00}}(\mathbf{q}\to\mathbf{0}) = \frac{1}{1+v_{\mathbf{0}}(\mathbf{q})\left|\mathbf{q}\right|^2\hat{\mathbf{q}}\cdot\mathbf{A}\hat{\mathbf{q}}}, \tag{5.14}$$

$$\varepsilon^{-1}_{\mathbf{G0}}(\mathbf{q}\to\mathbf{0}) = -\frac{\sqrt{v_{\mathbf{0}}(\mathbf{q})}\left|\mathbf{q}\right|\hat{\mathbf{q}}\cdot\mathbf{a}_{\mathbf{G}}}{1+v_{\mathbf{0}}(\mathbf{q})\left|\mathbf{q}\right|^2\hat{\mathbf{q}}\cdot\mathbf{A}\hat{\mathbf{q}}}, \tag{5.15}$$

$$\varepsilon^{-1}_{\mathbf{0G}}(\mathbf{q}\to\mathbf{0}) = -\frac{\sqrt{v_{\mathbf{0}}(\mathbf{q})}\left|\mathbf{q}\right|\hat{\mathbf{q}}\cdot\mathbf{b}_{\mathbf{G}}}{1+v_{\mathbf{0}}(\mathbf{q})\left|\mathbf{q}\right|^2\hat{\mathbf{q}}\cdot\mathbf{A}\hat{\mathbf{q}}}, \tag{5.16}$$

$$\varepsilon^{-1}_{\mathbf{GG'}}(\mathbf{q}\to\mathbf{0}) = B^{-1}_{\mathbf{GG}} + \frac{v_{\mathbf{0}}(\mathbf{q})\left|\mathbf{q}\right|^2(\hat{\mathbf{q}}\cdot\mathbf{a}_{\mathbf{G}})(\hat{\mathbf{q}}\cdot\mathbf{b}_{\mathbf{G'}})}{1+v_{\mathbf{0}}(\mathbf{q})\left|\mathbf{q}\right|^2\hat{\mathbf{q}}\cdot\mathbf{A}\hat{\mathbf{q}}}. \tag{5.17}$$

Now, we can combine the inverse dielectric function with the Coulomb potential again, to arrive at the final expression for the correlation part of the screened interaction

$$W^c_{\mathbf{00}}(\mathbf{q}\to\mathbf{0}) = -\left(v_{\mathbf{0}}(\mathbf{q})\left|\mathbf{q}\right|\right)^2\frac{\hat{\mathbf{q}}\cdot\mathbf{A}\hat{\mathbf{q}}}{1+v_{\mathbf{0}}(\mathbf{q})\left|\mathbf{q}\right|^2\hat{\mathbf{q}}\cdot\mathbf{A}\hat{\mathbf{q}}}, \tag{5.18}$$

$$W^c_{\mathbf{G0}}(\mathbf{q}\to\mathbf{0}) = -v_{\mathbf{0}}(\mathbf{q})\left|\mathbf{q}\right|\frac{\sqrt{v_{\mathbf{G}}(\mathbf{0})}\hat{\mathbf{q}}\cdot\mathbf{a}_{\mathbf{G}}}{1+v_{\mathbf{0}}(\mathbf{q})\left|\mathbf{q}\right|^2\hat{\mathbf{q}}\cdot\mathbf{A}\hat{\mathbf{q}}}, \tag{5.19}$$

$$W^c_{\mathbf{0G}}(\mathbf{q}\to\mathbf{0}) = -v_{\mathbf{0}}(\mathbf{q})\left|\mathbf{q}\right|\frac{\sqrt{v_{\mathbf{G}}(\mathbf{0})}\hat{\mathbf{q}}\cdot\mathbf{b}_{\mathbf{G}}}{1+v_{\mathbf{0}}(\mathbf{q})\left|\mathbf{q}\right|^2\hat{\mathbf{q}}\cdot\mathbf{A}\hat{\mathbf{q}}}, \tag{5.20}$$

$$W^c_{\mathbf{GG'}}(\mathbf{q}\to\mathbf{0}) = \sqrt{v_{\mathbf{G}}(\mathbf{0})v_{\mathbf{G'}}(\mathbf{0})}\left[B^{-1}_{\mathbf{GG'}} - \delta_{\mathbf{GG'}} + \frac{v_{\mathbf{0}}(\mathbf{q})\left|\mathbf{q}\right|^2(\hat{\mathbf{q}}\cdot\mathbf{a}_{\mathbf{G}})(\hat{\mathbf{q}}\cdot\mathbf{b}_{\mathbf{G'}})}{1+v_{\mathbf{0}}(\mathbf{q})\left|\mathbf{q}\right|^2\hat{\mathbf{q}}\cdot\mathbf{A}\hat{\mathbf{q}}}\right]. \tag{5.21}$$

5.1 2D Materials

5.1.1 Implementation to the *GW* Method

By inserting the 2D cutoff Coulomb potential from Eq. 4.2, we arrive at the analytical expressions in Eq. 4.11 to Eq. 4.14. In Fig. 5.1 we show the head component of the dielectric function, highlighting the impact of the 2D cutoff on its behavior. The dielectric function for bulk MoS_2 converges to a finite material-dependent value and exhibits a relatively flat behavior as $\mathbf{q}$ approaches zero. This justifies the assumption that the dielectric function does not depend on $\mathbf{q}$ in the long wavelength limit in 3D. In contrast, for the 2D case, a significant $\mathbf{q}$ dependence is observed: While for larger $\mathbf{q}$ values the dielectric function is similar to the bulk case, for smaller $\mathbf{q}$ it always approaches one, leading to a steep behavior for vanishing $\mathbf{q}$. This highlights the crucial role played by using an analytical expression to average the screened interaction, which captures the

intricate $\mathbf{q}$ dependence in a more accurate manner.

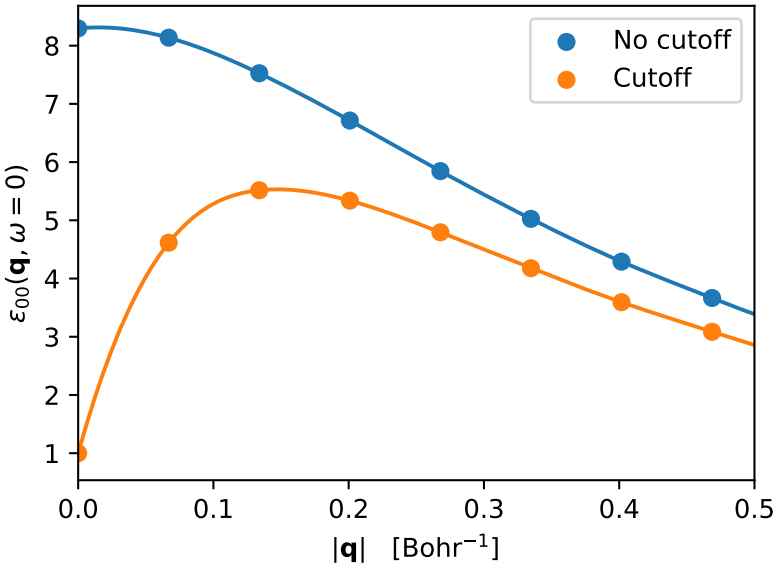

Figure 5.1: Dielectric function of MoS_2 with and without a 2D cutoff. The points are numerically calculated values, while the lines are splines to illustrate the $\mathbf{q}$ dependence for small $\mathbf{q}$.

Now we investigate the validity of the approximations made to derive the analytic expression. In Fig. 5.2, we compare the head of the dielectric function, the head of its inverse, and the final expression for the head of the screened potential with results from numeric calculations on a dense $\mathbf{q}$ grid. We can see that, in the limit of small q, the approximation to the dielectric function describes the numerical values outstandingly well. However, the inversion of the dielectric matrix worsens the quality. This is due to the fact, that also wing and body elements enter the head of the inverse, for which the quality of the approximation is expected to be worse, as they rely on a 1st (wings) or 0th (body) order approximations of the polarizability (see Eq. 3.53 to Eq. 3.55). The description of the screened potential is satisfactory because it is a product of the inverse dielectric function and the bare Coulomb potential, and evidently the Coulomb potential dominates, improving the overall result.

In Fig. 5.3, we investigate the head of the screened Coulomb potential in more detail, seeing again good agreement between numerical results and the analytical expression. In this figure, the orange bars represent a simple approximation to the integral over the first Brillouin zone. In principle, it would be possible to only use the $\mathbf{q} = \mathbf{0}$ value of the analytical expression for W^c_{00} (Eq. 4.15), corresponding to using the whole bar at

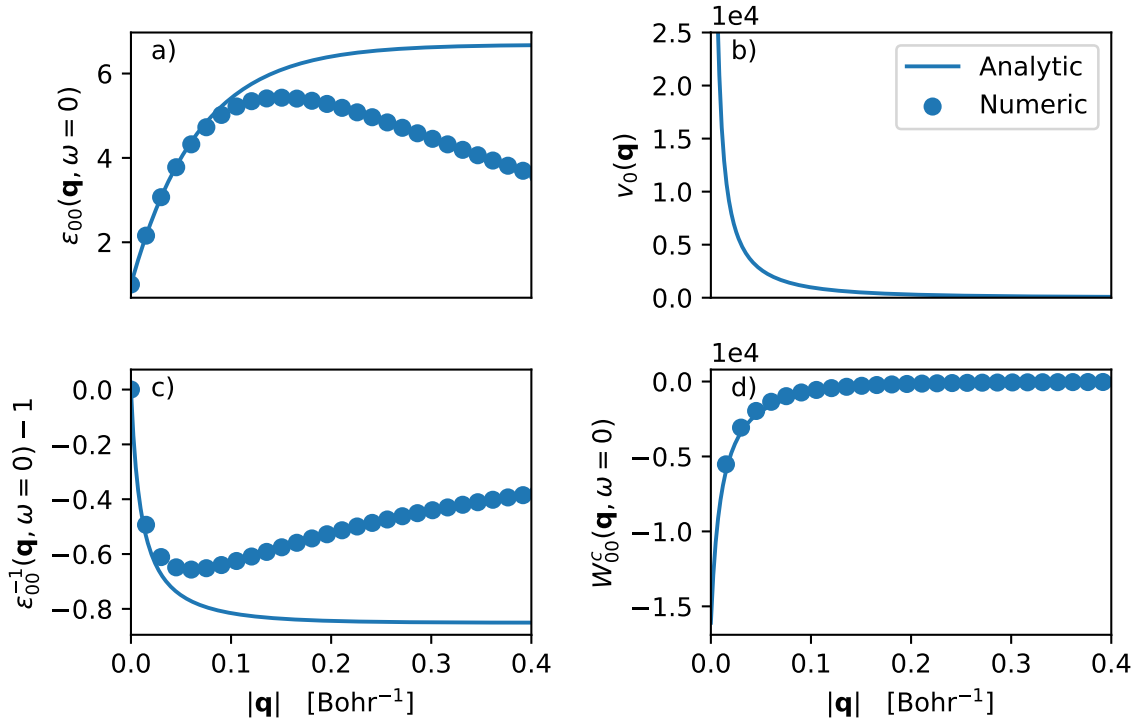

Figure 5.2: Components contributing to the screened interaction with a 2D cutoff for MoS_2: a) head of the dielectric function, b) 2D bare Coulomb potential, c) head of the inverse dielectric function minus one, d) head of the correlation part of the screened interaction. The dots represent the numerical results, while the lines represent the analytical expressions in the limit $\mathbf{q} \to \mathbf{0}$.

$\mathbf{q} = \mathbf{0}$. While the area under the curve is well approximated for larger $\mathbf{q}$ values where the function is flat, the bar at $\mathbf{q} = \mathbf{0}$ is a bad approximation for the area under the curve due to its steep convex behavior. Hence, we integrate the analytical expression over a small region Ω_0 around $\mathbf{q} = \mathbf{0}$ to cut out the gray area from the bar at this point. By using this procedure, the integral needs significantly less $\mathbf{q}$ points to be converged.

In order to perform the integration, we apply the integration procedure described in Ref. [3]. In more detail, the primitive cell is sampled regularly along the two basis vectors defining the 2D structure. This defines a new lattice represented by the blue points in Fig. 5.4. Now we define Ω_0 as the first Wigner-Seitz cell around $\mathbf{q} = \mathbf{0}$ with its volume being

$$\Omega_0 = \frac{\Omega_{BZ}}{N_{\mathbf{q}}}. \tag{5.22}$$

We introduce a new sub grid with $N_{q,\text{sub}}$ $\mathbf{q}$ points, represented by the orange dots, to

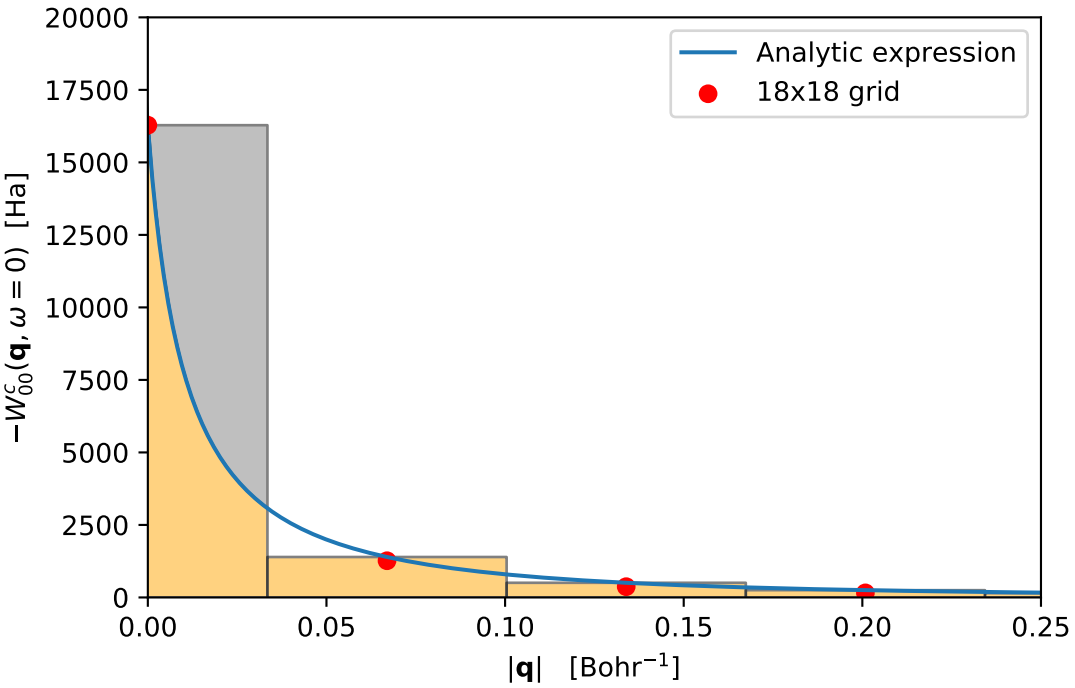

Figure 5.3: Head element of the correlation part of the screened Coulomb potential. The red dots represent the numerical results on a 18×18 $\mathbf{q}$ grid, while the lines represent the analytical expressions in the limit $\mathbf{q} \to \mathbf{0}$. The bars under the red dots represent the numeric approximation of the BZ integral.

sample the region Ω_0. In order to make the integration more efficient, we define a small circle $\Omega_{0,\text{sub}}$around $\mathbf{q} = \mathbf{0}$ on the sub grid with radius $r_{0,\text{sub}}$ (cf. Fig. 5.4 b))

$$r_{0,\text{sub}} = \sqrt{\frac{\Omega_0}{\pi N_{q,\text{sub}}}}. \tag{5.23}$$

On this circle we analytically integrate an approximation to Eq. 4.11. In more detail, we define the quantity $\mathbf{x} = \mathbf{q}L/2$ and the rotational average

$$A = \frac{1}{2\pi} \int_0^{2\pi} \hat{\mathbf{x}}(\varphi) \cdot \mathbf{A}\hat{\mathbf{x}}(\varphi) d\varphi. \tag{5.24}$$

With this, we can write the head of W^c as

$$W^c(2\mathbf{x}/L) = (2\pi L)^2 A\tilde{w}(\mathbf{x}) \tag{5.25}$$

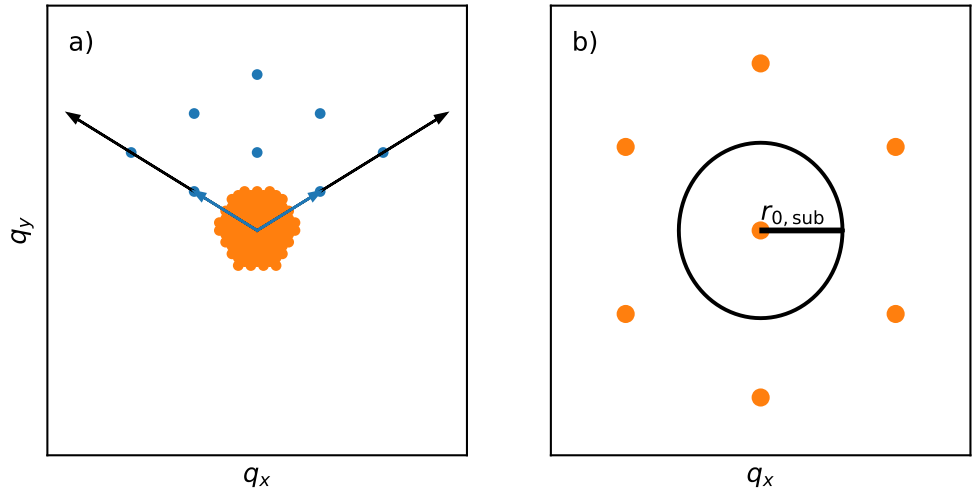

Figure 5.4: a) Sampling of the unit cell in reciprocal space. The black arrows represent the basis vectors and the blue points a 3×3 grid. The blue arrows define a new sub-lattice, whose Brillouin zone is sampled with the orange points. b) Zoom into the region of the orange points in a): Around $\mathbf{q} = \mathbf{0}$, we define a circle with radius $r_{0,\mathrm{sub}}$ for an analytic approximation of the integral.

with the simplified function

$$\tilde{w}(\mathbf{x}) = -\left(\frac{1 - e^{-|\mathbf{x}|}}{|\mathbf{x}|}\right)^2 \frac{1}{1 + 4\pi A\left(1 - e^{-|\mathbf{x}|}\right)}. \tag{5.26}$$

For small $\mathbf{x}$, we use the Padé approximation of this function

$$\tilde{w}(\mathbf{x}) \approx -\frac{1}{1 + (1 + 4\pi A)\,|\mathbf{x}|}, \tag{5.27}$$

leading to the following approximated analytical integral on the circle around $\mathbf{q} = \mathbf{0}$

$$\int_{\Omega_{0,\mathrm{sub}}} \tilde{w}(\mathbf{x}) d\mathbf{x} \approx \frac{-2\pi\left(4\pi A r_{0,\mathrm{sub}} + r_{0,\mathrm{sub}} - \ln\left(4\pi A r_{0,\mathrm{sub}} + r_{0,\mathrm{sub}} + 1\right)\right)}{(4\pi A + 1)^2}. \tag{5.28}$$

In Fig. 5.5 we see that this method leads to an improved convergence of the numerical integral. Hence, it will be used as the standard method throughout this thesis.

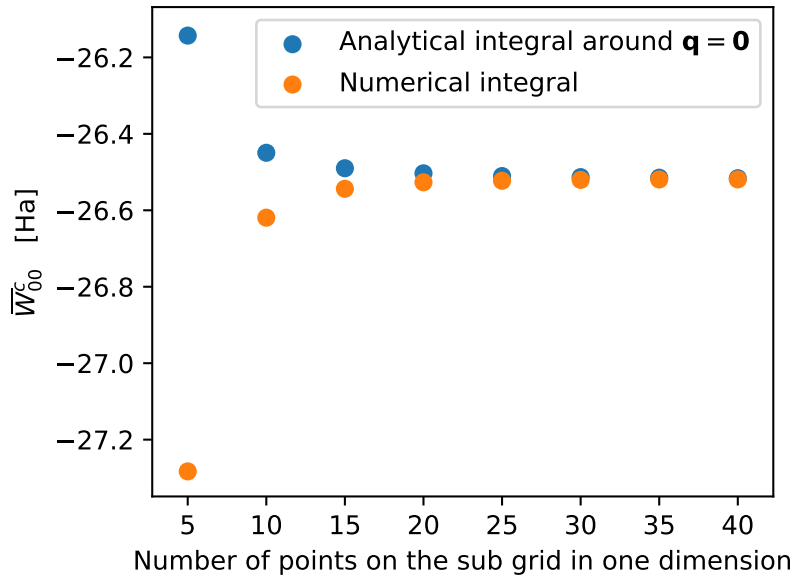

Figure 5.5: Integral of the head of the correlation part of the screened Coulomb potential around $\mathbf{q} = \mathbf{0}$. The blue points represent the method presented in the text, whilst the orange points come from a numerical sum for the integration. Here, we introduced the abbreviation $\overline{W}^c_{00} \equiv \frac{1}{\Omega_0} \int_{\Omega_0} W^c_{00}(\mathbf{q}, \omega = 0) \mathrm{d}\mathbf{q}$.

5.1.2 Implementation to the BSE

After having discussed the implementation to GW, we now investigate the necessary changes to achieve an implementation to the BSE. The direct term of the BSE Hamiltonian is originally expressed in terms of the complete screened interaction, encompassing both its correlation part and the bare potential. As the bare Coulomb potential is diagonal in the plane wave basis, the only difference will appear in the diagonal elements

$$W_{\mathbf{00}}(\mathbf{q} \to \mathbf{0}) = \frac{4\pi \left(1 - e^{-|\mathbf{q}|L/2}\right)}{|\mathbf{q}|^2} \frac{1}{1 + 4\pi \left(1 - e^{-\mathbf{q}L/2}\right) \hat{\mathbf{q}} \cdot \mathbf{A}\hat{\mathbf{q}}} \tag{5.29}$$

$$W_{\mathbf{GG'}}(\mathbf{q} \to \mathbf{0}) = \sqrt{v_{\mathbf{G}}(\mathbf{0}) v_{\mathbf{G'}}(\mathbf{0})} \left[B^{-1}_{\mathbf{GG'}} + \frac{4\pi \left(1 - e^{-|\mathbf{q}|L/2}\right) (\hat{\mathbf{q}} \cdot \mathbf{a}_{\mathbf{G}}) (\hat{\mathbf{q}} \cdot \mathbf{b}_{\mathbf{G'}})}{1 + 4\pi \left(1 - e^{-|\mathbf{q}|L/2}\right) \hat{\mathbf{q}} \cdot \mathbf{A}\hat{\mathbf{q}}} \right]. \tag{5.30}$$

The wings are the same for the correlation part and also the modification of the expression for the body is rather small, since we just have to leave away the Kronecker delta when comparing to Eq. 5.21. However, the head element of the full screened interaction diverges when including the bare Coulomb potential. This divergence makes it challenging to converge the numerical integral of the head element. Hence, we propose another

approach, where we make use of the formula of the head of the correlation part. We write the screened interaction as a sum of its correlation part and the Coulomb potential

$$W = W^c + v. \tag{5.31}$$

By doing so, we can perform the integral over the bare Coulomb potential analytically. For the correlation part, we can use the GW implementation to compute the integral numerically. With this idea, we are able to converge the integral much faster as one can see in Fig. 5.6. Even for a sub grid of 225×225, the integration of the full screened interaction does not look fully converged, while the new approach converges significantly faster.

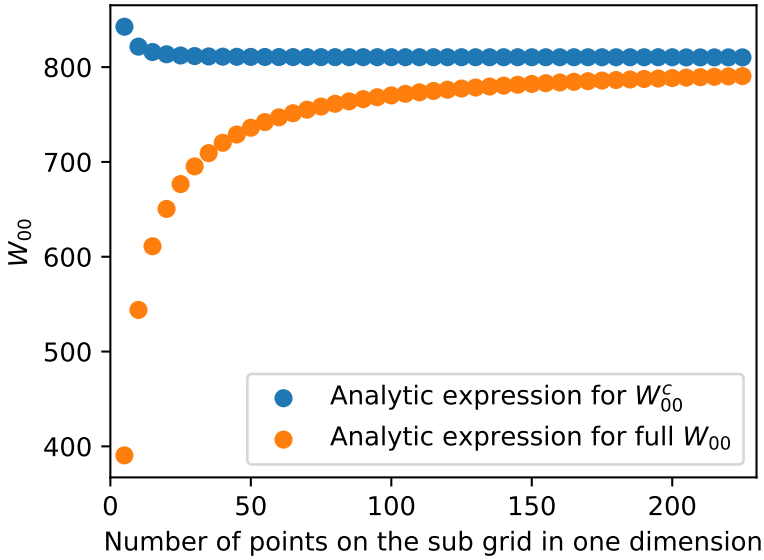

Figure 5.6: Integral of the head of the full screened interaction in the BSE implementation. The convergence with respect to the number of $\mathbf{q}$ points is investigated for the two different methods described in the text. Here, we introduced the abbreviation $\overline{W}_{00} \equiv \frac{1}{\Omega_0}\int_{\Omega_0} W_{00}(\mathbf{q}, \omega = 0)\mathrm{d}\mathbf{q}$.

5.2 1D Materials

5.2.1 Implementation to the GW Method

For a 1D cutoff, there is no closed expression of the Coulomb potential (cf. Eq. 4.5). Consequently, there is also no closed expression for the screened Coulomb potential.

However, it is still possible to evaluate the numeric expression and insert it in Eq. 5.18 to Eq. 5.21. Using the divergent term from Eq. 4.7, we can see that the exact limit of the head becomes

$$W^c_{\mathbf{00}}(\mathbf{q} = \mathbf{0}) = 0. \tag{5.32}$$

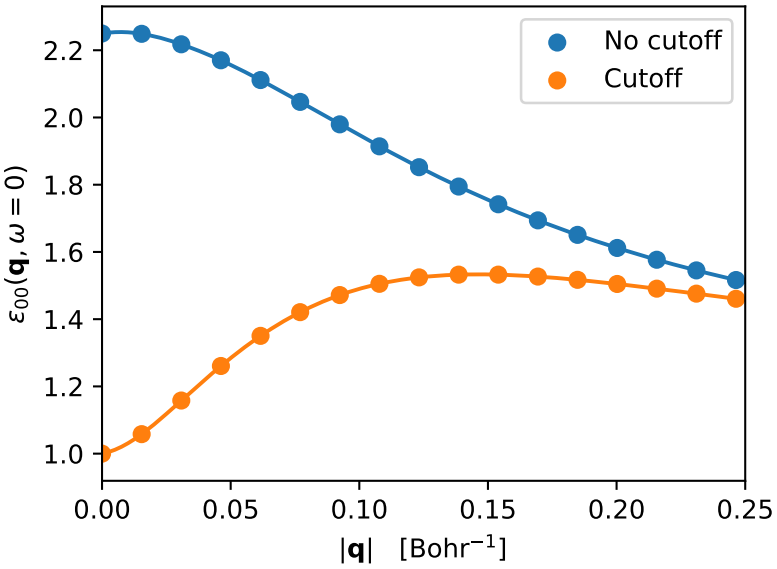

Figure 5.7: Dielectric function of PPP with a 1D cutoff.

Like in the case of the 2D cutoff, we display the head of the dielectric function, it's inverse, and the screened Coulomb interaction in Fig. 5.8. Since the unit cell of the later investigated material contains too many atoms, we introduce a toy model here, in order to be able to calculate the numerical values on a dense enough $\mathbf{q}$ grid. This model consists of a chain, where a hydrogen dimer is alternating with one vacancy. This system is used, because it is expected to have a band gap and has only two atoms per unit cell, making it feasible to go to larger grids.

The head element of the dielectric function is described very well by the analytic formula, just as well as in the 2D case in Fig. 5.2. We can also see that the description of the head element of the inverse dielectric function is worse. One problem here is, that the values of the function in Fig. 5.8 c) are very small, meaning that the relative error grows. After multiplication with the Coulomb potential, the relative error is inherited by the screened interaction. This explains, why the overall description of the screened interaction looks worse than in the 2D case. However, for small $\mathbf{q}$ values it still seems to be sufficient, such that we implement a procedure analogous to the 2D case.

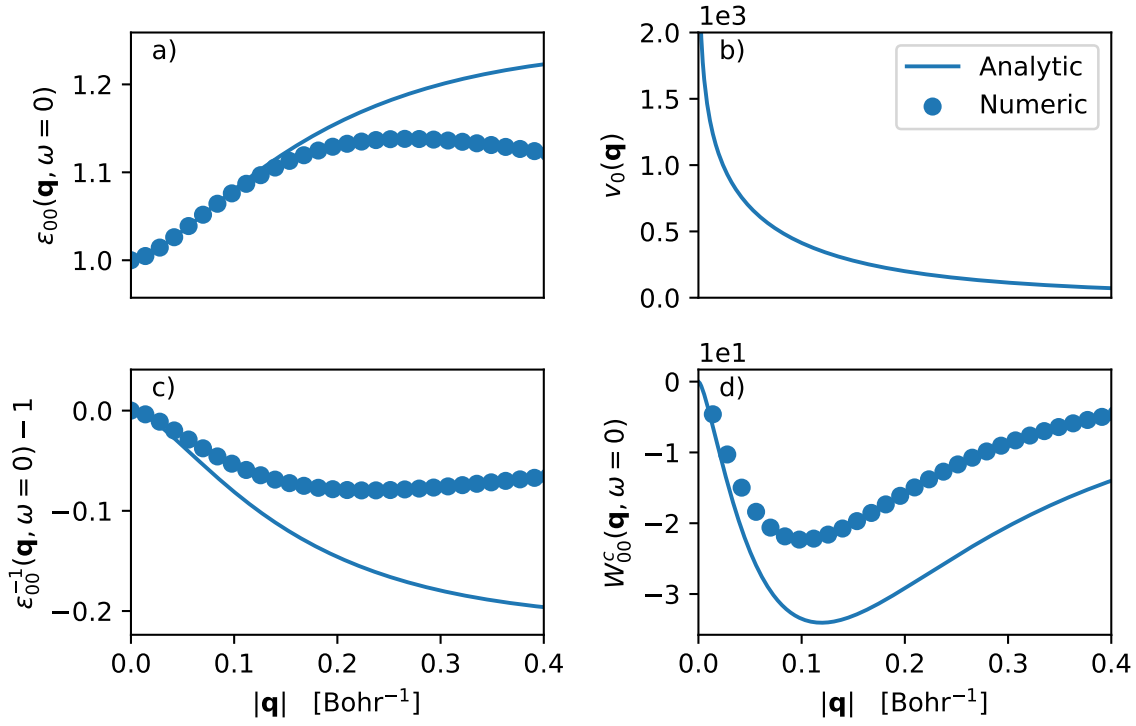

Figure 5.8: Components contributing to the screened interaction with a 1D cutoff: a) head of the dielectric function, b) 1D bare Coulomb potential, c) head of the inverse dielectric function minus one, d) head of the correlation part of the screened interaction. The dots represent the numerical results, while the lines represent the analytical expressions in the limit $\mathbf{q} \to \mathbf{0}$.

The $\mathbf{q}$ sampling of the 1D Brillouin is much simpler, making the integration easier in this case. The volume one $\mathbf{q}$ point has is given by

$$\Omega_0 = \frac{2\pi}{aN_{\mathbf{q}}}. \tag{5.33}$$

Where a is the lattice parameter in the periodic z-direction. For the averaging we now evenly sample between $-\frac{\pi}{aN_{\mathbf{q}}}$ and $\frac{\pi}{aN_{\mathbf{q}}}$ to sum up the contributions to the screened interaction. Compared to the 2D case, the integration is also simpler, because the screened Coulomb potential is not as steep for $\mathbf{q} \to 0$. In Fig. 5.9, one can see that the integral converges quickly, indicating that no sophisticated method, as required in the 2D case, is necessary.

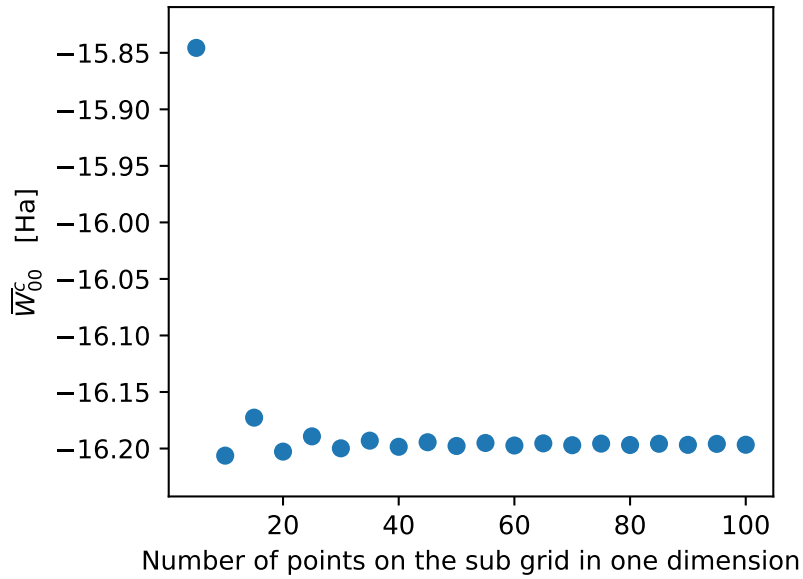

Figure 5.9: Integral of the head of the correlation part of the screened Coulomb potential around $\mathbf{q} = \mathbf{0}$. Here, we introduced the abbreviation $\overline{W}^c_{00} \equiv \frac{1}{\Omega_0}\int_{\Omega_0} W^c_{00}(\mathbf{q}, \omega = 0)\mathrm{d}\mathbf{q}$.

5.2.2 Implementation to the BSE

For the full screened interaction used in the BSE implementation, we apply the same method as in the 2D case. We make use of the *GW* implementation of the correlation part of the screened interaction and add the averaged bare Coulomb potential afterwards.

5.3 0D Materials

Finally, we discuss the type of materials with the lowest possible dimension, 0D materials. This scenario differs slightly from the previous cases, since it lacks periodicity in real space along any direction. Consequently, there exists only a single $\mathbf{q}$ point in reciprocal space, eliminating the continuous $\mathbf{q}$ variable seen in previous cases. Therefore, we insert

the expression from Eq. 4.10 and arrive at the following limits for $\mathbf{q} = \mathbf{0}$

$$W^c_{\mathbf{00}}(\mathbf{q} = \mathbf{0}) = 0, \tag{5.34}$$

$$W^c_{\mathbf{G0}}(\mathbf{q} = \mathbf{0}) = 0, \tag{5.35}$$

$$W^c_{\mathbf{0G}}(\mathbf{q} = \mathbf{0}) = 0, \tag{5.36}$$

$$W^c_{\mathbf{GG'}}(\mathbf{q} = \mathbf{0}) = \sqrt{v_{\mathbf{G}}(\mathbf{0}) v_{\mathbf{G'}}(\mathbf{0})} \left[B^{-1}_{\mathbf{GG'}} - \delta_{\mathbf{GG'}}\right]. \tag{5.37}$$

It was previously mentioned, that in the current implementation in `exciting` the zero elements of the screened interaction were left out. Looking at Eq. 5.34 to Eq. 5.37, it is evident that in the 0D case both methods are equivalent. Hence, 0D materials are not further investigated in this thesis.

6 Computational Results

6.1 2D Materials

6.1.1 *GW* Results

The two 2D materials investigated in this thesis are molybdenum disulfide (MoS_2) and hexagonal boron nitride (h-BN). Both materials have relatively simple structures, each consisting of a hexagonal lattice, with three atoms per unit cell for MoS_2 and two atoms per unit cell for h-BN. Even though their structure is similar, both materials exhibit distinctive electronic properties. While MoS_2 can be classified as a semiconductor with a direct band gap, h-BN is an insulator with an indirect band gap [13].

The structures of both materials have been relaxed with the PBE functional in previous works [14, 15]. Their ground states have been calculated with PBE using a 30×30×1 **k** grid.

Table 6.1: Computational parameters for the investigated 2D materials MoS_2 and h-BN.

Material	Lattice constant	Vacuum	DFT functional	Empty states
MoS_2	3.1858 Å	30 Bohr	PBE	400
h-BN	2.5170 Å	30 Bohr	PBE	400

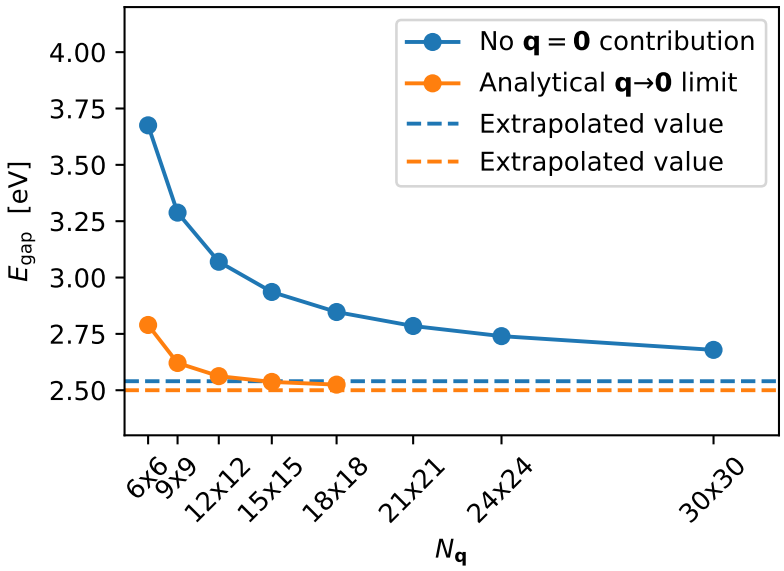

Figure 6.1: Direct band gap at K of MoS_2 calculated with G_0W_0. The $\mathbf{q}$ grids range from 6×6×1 to 18×18×1 for the implementation with the analytical screened interaction and up to 30×30×1 for the old implementation. The respective extrapolated band gap is depicted with the corresponding color.

Applying the procedure described in Sec. 5.1 in the G_0W_0 approximation yields satisfactory results for MoS_2. Using a $\mathbf{q}$ grid of 18×18×1, we find a direct band gap of 2.52 eV at the high symmetry point K. In [3], a value of 2.54 eV was calculated using PBE for the structure relaxation and the ground state. In Fig. 6.1, one can see the convergence behavior of the band gap with respect to the number of $\mathbf{q}$ points. The blue points represent the old implementation in `exciting` and are taken from [15], while the orange points represent the new implementation using the analytic expression. From this plot we can see that with the new method the result is well converged within 0.05 eV using an 18×18×1 $\mathbf{q}$ grid. On the other hand, the old method drastically overestimates the gap for small numbers of $\mathbf{q}$ points and converges much slower. Unfortunately, it was not feasible to go to larger $\mathbf{q}$ grids within the scope of this thesis. To better compare the results in the limit of a large number of $\mathbf{q}$ points, we extrapolate the band gap for both methods with a function of the form:

$$E_g(N_{\mathbf{q}}) = E_\infty + \frac{A}{B + N_{\mathbf{q}}}. \tag{6.1}$$

This yields values of $E_\infty^{\text{new}} = 2.50$ eV for the new method including the analytical $\mathbf{q} \to \mathbf{0}$

limit and $E_{\infty}^{\text{old}} = 2.54$ eV for the old method without $\mathbf{q} = \mathbf{0}$ contribution. So both methods agree well within a tolerance of 0.05 eV. For comparision, an experimental value of 2.5 eV was reported in [3]. However, one has to keep in mind, that the structure relaxed with the PBE functional does not perfectly agree with the experimental structure, meaning that experiment and theory cannot be compared straightforwardly. The issue of the dependence of the band gap of MoS_2 on the structure is extensively discussed in [15].

In the case of h-BN we calculate an indirect band gap ($K \to \Gamma$) of 6.75 eV with a $\mathbf{q}$ grid of 18×18×1. This lies well within a reported range of 6.00-7.32 eV [13]. Similar to the case of MoS_2, we can also see a great improvement in the convergence of the gap in Fig. 6.2 compared to the previous implementation. We don't have reference data to the same extent as for MoS_2, so we cannot compare the values of the gaps in a larger limit for the number of $\mathbf{q}$ points. However, the improved convergence makes the results overall satisfactory.

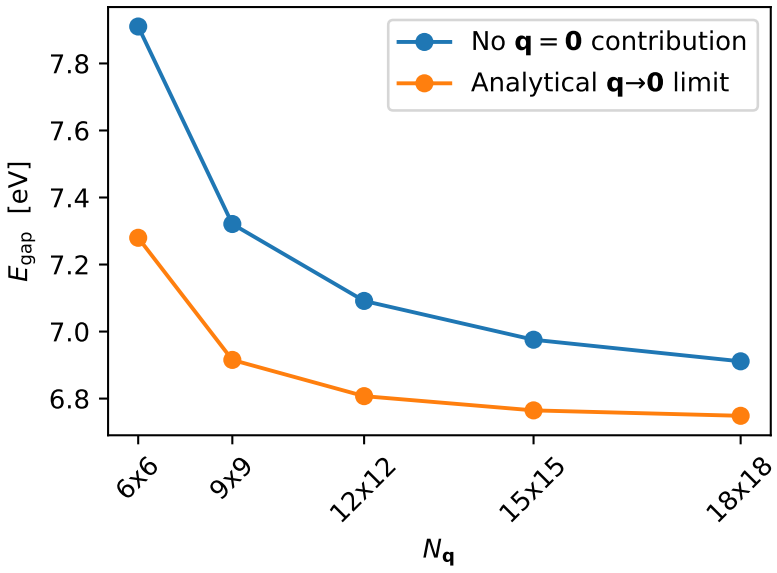

Figure 6.2: Indirect band gap at $K \to \Gamma$ of h-BN calculated with G_0W_0. The $\mathbf{q}$ grids range from 6×6×1 to 18×18×1 for both implementations.

6.1.2 BSE Results

Continuing with the discussion of excited state properties, the 2D Coulomb cutoff was implemented into the `exciting` code. In Fig. 6.3 one can see the absorption spectrum

of MoS_2 calculated with and without a cutoff. The overall shape of the spectrum looks reasonable when comparing with results from [16]. The only difference is that in our case we do not see a splitting of the first peak, because spin-orbit coupling was not applied [17]. It is evident that the primary effect of the cutoff is a rigid shift of the spectrum towards lower energies. Notably, the overall effect of the cutoff is significantly smaller compared to its impact in *GW* calculations. Nevertheless, its implementation remains essential to ensure that both *GW* and BSE calculations are performed on a consistent theoretical basis.

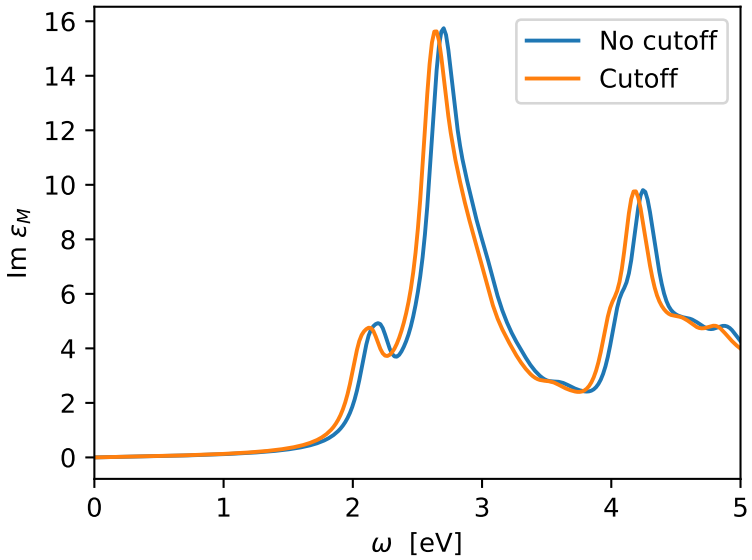

Figure 6.3: Imaginary part of the dielectric function of MoS_2 calculated with the BSE. The spectra were calculated with and without a cutoff using a 45×45×1 $\mathbf{q}$ grid.

After discussing the general impact of the cutoff on the spectrum, our focus now shifts to examining the performance of averaging the analytical expression of the screened interaction. In Fig. 6.4, we illustrate the convergence behavior of the exciton binding energy E_b with respect to the number of $\mathbf{q}$ points. Three distinct methods are employed for comparison:

1. The binding energy is calculated without using a cutoff.
2. The calculation is performed with a cutoff, but the screening for $\mathbf{q} \to 0$ is not adapted, i.e. a 3D limit is taken. (This corresponds to the old implementation.)

3. The 2D analytic treatment for $\mathbf{q} \to 0$ is employed.

The curve with the cutoff and using the exact 2D limit is nicely converged with a 33×33×1 grid and exhibits a flat behavior when increasing the grid up to 60×60×1. On the other hand, the curve with cutoff using 3D screening and the curve without cutoff do not converge satisfactorily within the range of $\mathbf{q}$ points considered. This observation emphasizes the importance of not only introducing a cutoff but also applying an appropriate treatment to address the singularity of the screened interaction. The numerical value for the exciton binding energy, calculated with the 2D screening, is 0.47 eV. This result is in good agreement with previously reported values, e.g. 0.54 eV in [16]. The plot clearly illustrates a significant improvement over the old implementation, which consistently underestimates the binding energy.

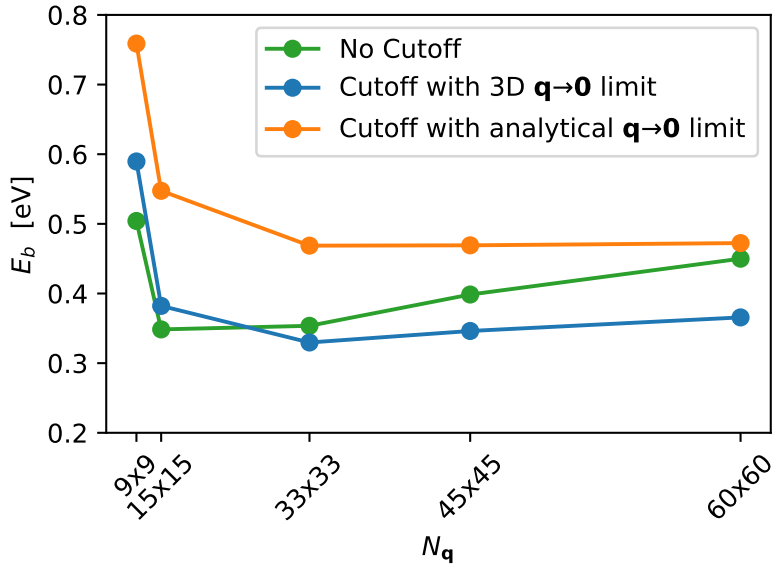

Figure 6.4: Binding energy of the lowest-lying exciton in MoS_2 calculated with the BSE based on G_0W_0 applying three different procedures. The $\mathbf{q}$ grids range from 9×9×1 to 60×60×1.

The spectra for h-BN are plotted in Fig. 6.5, where one can see that the effect of the cutoff is again a rigid shift. It is significantly larger than for MoS_2. The spectral shape is very similar to previously calculated spectra [18, 13].

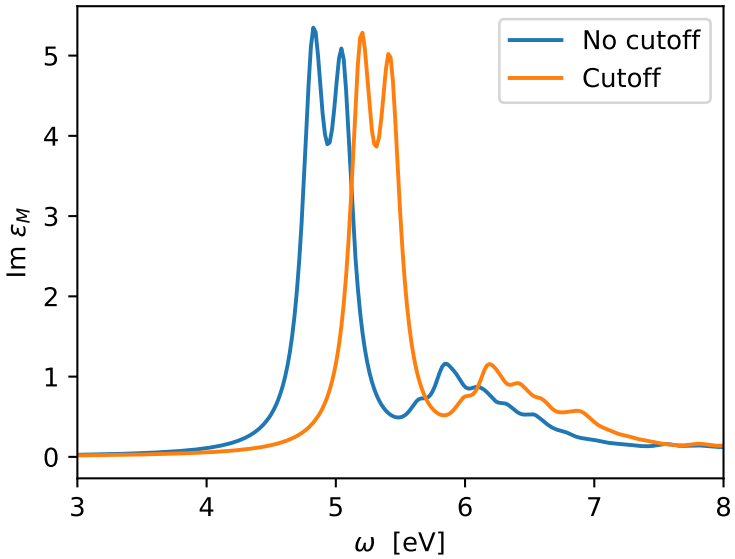

Figure 6.5: Imaginary part of the dielectric function of h-BN calculated with the BSE. The spectra were calculated with and without cutoff and a $\mathbf{q}$ grid of 45×45×1.

Finally, the convergence of the exciton binding energy is shown in Fig. 6.6 for the three different methods. The binding energy does not converge for the case of no applied cutoff within the considered number of $\mathbf{q}$ points, which means that the cutoff is even more important than in the case of MoS_2. With cutoff and the analytic treatment of the $\mathbf{q} \to 0$ singularity, the curves look well converged. The final value of the binding energy $E_b = 2.06$ eV lies well within the range of $1.50 - 2.19$ eV reported in [13].

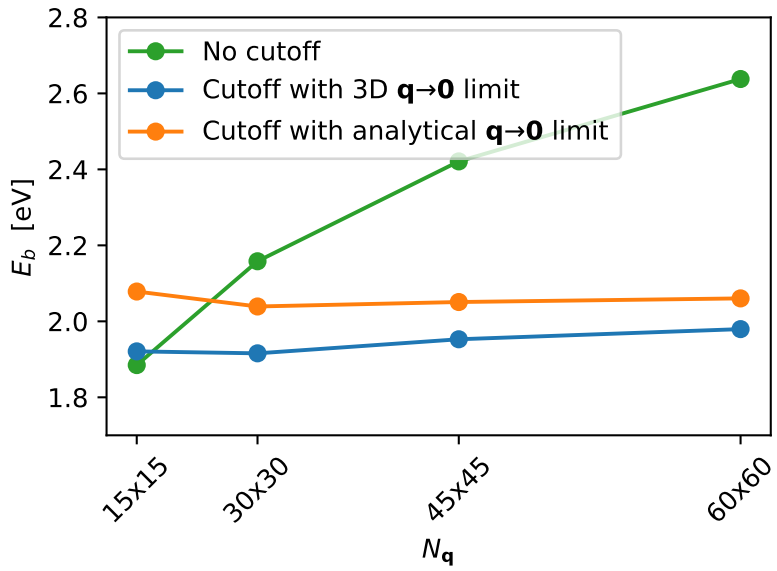

Figure 6.6: Binding energy of the lowest-lying exciton in h-BN calculated with the BSE based on G_0W_0 applying three different procedures. The $\mathbf{q}$ grids range from 15×15×1 to 60×60×1.

6.2 1D Materials

6.2.1 *GW* Results

The 1D material investigated in this thesis is poly(*para*-phenylene) (PPP). We assume that the polymer consists of infinitely repeated units of phenylene rings. The system does not exhibit a torsion angle between adjacent phenylene units, which reduces the computational cost. The structure was previously relaxed in our research group using the PBE functional[19]. Using the method described in Sec. 5.2, we calculated the band gap with an applied 1D cutoff. In Fig. 6.7, we compare the results of the old and the new implementation. As in the 2D case, the new one represents an improvement, making the band gap converge faster with respect to the number of $\mathbf{q}$ points. However, the overall improvement is not as drastic as before. This can be explained as follows: Due to the further reduced dimensionality, the screening weakens, resulting in a lower overall contribution of the correlation part of the self-energy Σ^c. Hence, the correction achieved by our method also becomes weaker. The calculated value of $E_g = 4.23$eV is in reasonable agreement with values from [20], even though a precise comparison is difficult because we don't include the torsion angle in our calculation.

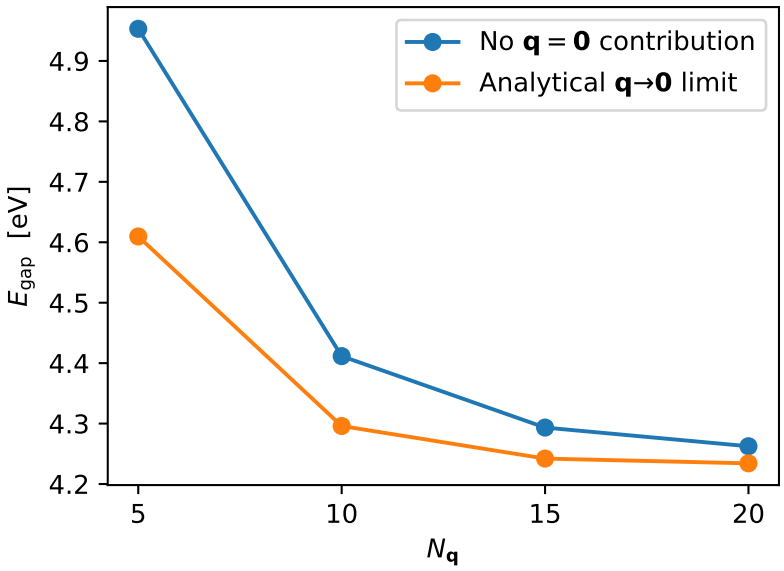

Figure 6.7: Direct band gap of PPP at Γ calculated with G_0W_0 with and without cutoff. The **q** grids range from 1×1×5 to 1×1×20 for both methods.

6.2.2 BSE Results

In the BSE implementation of `exciting`, there was previously no option for a 1D Coulomb truncation. Hence, it had to be implemented together with the correct analytical treatment of the singularity. In Fig. 6.8 we can see that the effect of the 1D cutoff is very similar to the 2D case: It mainly shifts the spectrum without drastically changing its shape. However, there is a small difference in the third peak, which appears a little wider with the cutoff.

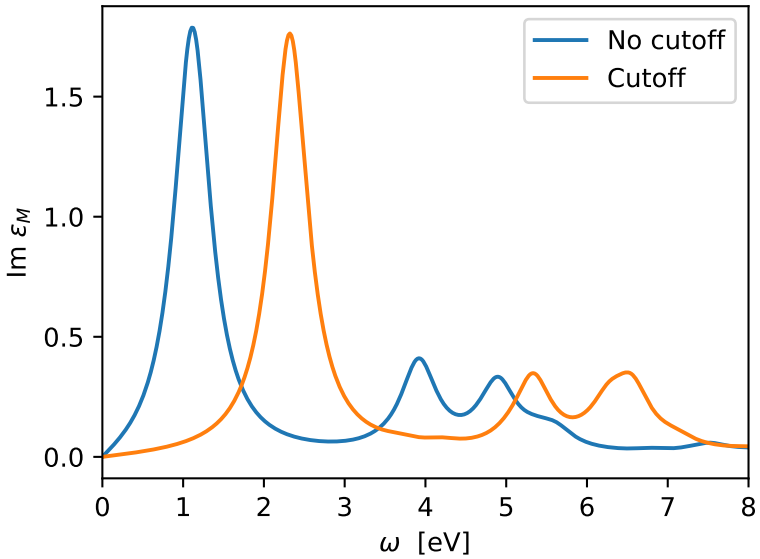

Figure 6.8: Imaginary part of the dielectric function of PPP calculated with the BSE. The spectra were calculated with and without a cutoff using a $1\times1\times20$ $\mathbf{q}$ grid.

In Fig. 6.9 one can see the exciton binding energy plotted against the number of $\mathbf{q}$ points for the three different implementations. Without cutoff, the binding energy diverges and becomes even larger than the band gap for large number of $\mathbf{q}$ points. This might be due to the relatively small vacuum size of 20 Bohr in x and y direction. The influence of the analytical $\mathbf{q} \to \mathbf{0}$ limit is hard to investigate, as its effect is on a different scale than the one of the cutoff.

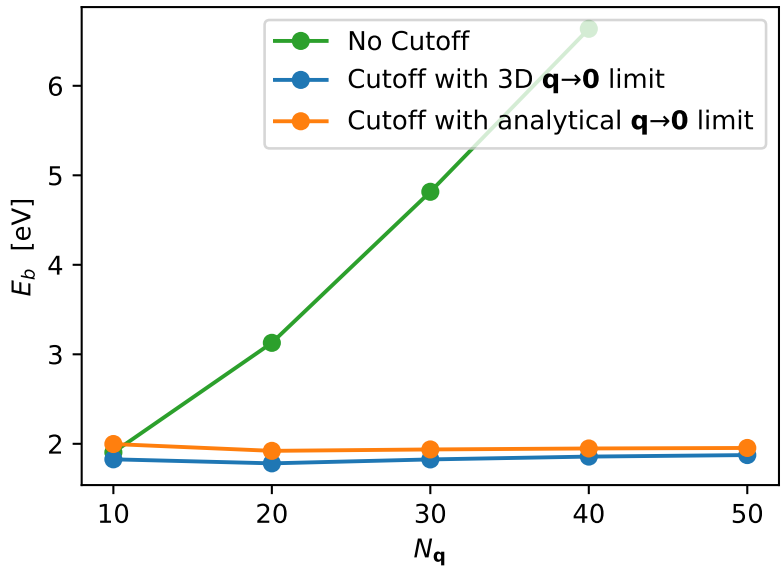

Figure 6.9: Binding energy of the lowest-lying exciton in PPP calculated with the BSE based on G_0W_0 applying three different procedures. The $\mathbf{q}$ grids range from $1\times1\times10$ to $1\times1\times50$. The vacuum in x and y direction is 20 Bohr.

Therefore, in Fig. 6.10 only the values obtained by using a cutoff are compared with the 3D limit. The analytical limit yields further improvement, since the binding energy converges faster than with the 3D limit. Overall, the latter approaches the curve with the analytical limit for a large number of $\mathbf{q}$ points. The final value of $E_b = 1.95$ eV is in good agreement with values found in [20].

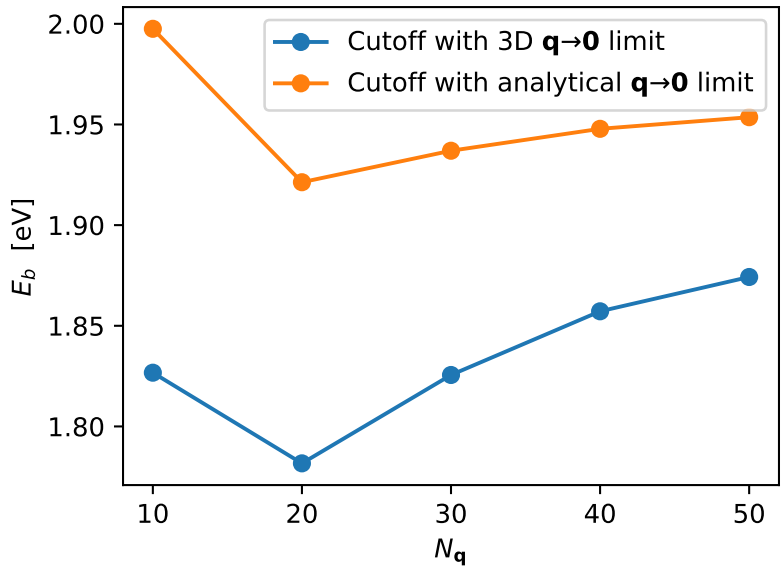

Figure 6.10: Binding energy of the lowest-lying exciton in PPP calculated with the BSE based on G_0W_0. Same results as in Fig. 6.9 but without the values for no applied cutoff.

The fact that in the case of no applied Coulomb cutoff the binding energy is becoming larger than the band gap (i.e. the first exciton energies are negative) is clearly indicating numerical difficulties, which might arise due to interaction between the periodically repeated images. Therefore, we investigate in Fig. 6.11, whether increasing the vacuum improves this issue. We can see that for varying vacuum, the values with cutoff are constant, which meets our expectations. Also the values without Coulomb truncation approach the values with Coulomb cutoff in the limit of large vacuum. However, even larger vacuum sizes would be needed to solves the issue. Unfortunately, the ground state calculations with larger vacuum were hard to converge, such that it was not possible to increase the vacuum further.

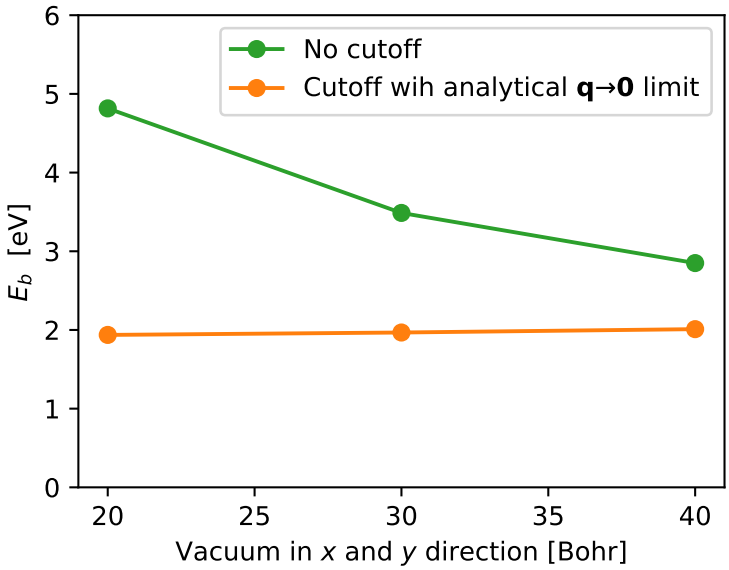

Figure 6.11: Binding energy of the lowest-lying exciton in PPP calculated with the BSE based on G_0W_0 with and without cutoff. Here, the vacuum is varied with a fixed $\mathbf{q}$ grid of $1\times1\times30$.

7 Conclusions

The first goal of this thesis was, to make *GW* calculations with a 2D cutoff more efficient by implementing the analytical limits for the screened interaction as presented in Ref. [3] in `exciting`. This goal was successfully achieved, as demonstrated in the case of MoS_2. In comparison to previous calculations that utilized larger $\mathbf{q}$ point grids, we applied the analytical limits and achieved superior precision in the band gap calculations. More specific, using a 12×12×1 $\mathbf{q}$ grid, we attained a higher level of precision than with the older implementation with a 30×30×1 $\mathbf{q}$ grid. Also for h-BN, we observed a significant improvement of convergence speed.

Then, we aimed at extending the analytical method from the case of a 2D cutoff to a 1D cutoff. The example of PPP demonstrated that, we could achieve also in this case an improvement in terms of convergence. While it was not as drastic as in the 2D case, it still presented a noticeable difference.

The final objective was, to extend the approach to the BSE. Previously, there was no cutoff implemented within the `exciting` BSE framework. The incorporation of a 2D cutoff had a significant impact on the convergence of the exciton binding energy of h-BN. Implementing a 1D cutoff, we could as well observe a significant speedup as shown for the exciton binding energy of PPP. The implementation of the analytical limits of the screened Coulomb potential improved the results further. For instance, in the case of MoS_2, the exciton binding energy converged much faster. With our correction we were able to correct the binding energy by around 100 meV, which lead to better agreement with theoretical literature values.

In summary, all goals of this thesis could be achieved. Overall, they makes low-dimensional MBPT calculations easier to converge with respect to the number of $\mathbf{q}$ points and the vacuum size. This opens a wide range of possibilities to compute more complex low-dimensional materials within the `exciting` code.

Bibliography

[1] Andris Gulans et al. "exciting: a full-potential all-electron package implementing density-functional theory and many-body perturbation theory". In: *Journal of Physics: Condensed Matter* 26.36 (Aug. 2014), p. 363202. DOI: 10.1088/0953-8984/26/36/363202. URL: https://dx.doi.org/10.1088/0953-8984/26/36/363202.

[2] Sohrab Ismail-Beigi. "Truncation of periodic image interactions for confined systems". In: *Phys. Rev. B* 73 (23 June 2006), p. 233103. DOI: 10.1103/PhysRevB.73.233103. URL: https://link.aps.org/doi/10.1103/PhysRevB.73.233103.

[3] Filip Anselm Rasmussen et al. "Efficient many-body calculations for two-dimensional materials using exact limits for the screened potential: Band gaps of MoS 2 , h-BN, and phosphorene". In: (2016). URL: https://journals.aps.org/prb/abstract/10.1103/PhysRevB.94.155406.

[4] Richard M. Martin, Lucia Reining, and David M. Ceperley. *Interacting Electrons: Theory and Computational Approaches*. Cambridge University Press, 2016. DOI: 10.1017/CBO9781139050807.

[5] Hedin, Lars. "New Method for Calculating the One-Particle Green's Function with Application to the Electron-Gas Problem". eng. In: Physical Review series I 139.3A (1965), 796–823. ISSN: 0031-899X. URL: %7Bhttps://lup.lub.lu.se/search/files/5381803/8835242.pdf%7D.

[6] Lars Hedin and Stig O. Lundqvist. "Effects of Electron-Electron and Electron-Phonon Interactions on the One-Electron States of Solids". English. In: *Solid State Physics*. Ed. by Frederick Seitz, David Turnbull, and Henry Ehrenreich. Vol. 23. doi:10.1016/S0081-1947(08)60615-3. United States: Academic Press, 1969, pp. 1–181. ISBN: 978-0-12-607723-0. DOI: 10.1016/S0081-1947(08)60615-3.

[7] Hong Jiang et al. "FHI-gap : A GW code based on the all-electron augmented plane wave method". In: (2012). URL: https://www.sciencedirect.com/science/article/pii/S0010465512003049.

[8] Mark S. Hybertsen and Steven G. Louie. "Electron correlation in semiconductors and insulators: Band gaps and quasiparticle energies". In: *Phys. Rev. B* 34 (8 Oct. 1986), pp. 5390–5413. DOI: 10.1103/PhysRevB.34.5390. URL: https://link.aps.org/doi/10.1103/PhysRevB.34.5390.

[9] Peter Puschnig. "Excitonic Effects in Organic Semi-Conductors - An Ab-initio Study within the LAPW Method". PhD thesis. Jan. 2002.

[10] Christoph Freysoldt et al. "Dielectric anisotropy in the GW space–time method". In: (2007). URL: https://www.sciencedirect.com/science/article/abs/pii/S0010465506003134.

[11] Jun Yan et al. "Linear density response function in the projector augmented wave method: Applications to solids, surfaces, and interfaces". In: (2011). URL: https://journals.aps.org/prb/abstract/10.1103/PhysRevB.83.245122.

[12] Stephan Sagmeister and Claudia Ambrosch-Draxl. "Time-dependent density functional theory versus Bethe–Salpeter equation: an all-electron study". In: *Phys. Chem. Chem. Phys.* 11 (22 2009), pp. 4451–4457. DOI: 10.1039/B903676H. URL: http://dx.doi.org/10.1039/B903676H.

[13] F. Ferreira et al. "Excitons in hexagonal boron nitride single-layer: a new platform for polaritonics in the ultraviolet". In: *J. Opt. Soc. Am. B* 36.3 (Mar. 2019), pp. 674–683. DOI: 10.1364/JOSAB.36.000674. URL: https://opg.optica.org/josab/abstract.cfm?URI=josab-36-3-674.

[14] Qiang Fu, Dmitrii Nabok, and Claudia Draxl. "Energy-Level Alignment at the Interface of Graphene Fluoride and Boron Nitride Monolayers: An Investigation by Many-Body Perturbation Theory". In: *The Journal of Physical Chemistry C* 120.21 (2016), pp. 11671–11678. DOI: 10.1021/acs.jpcc.6b01741. eprint: https://doi.org/10.1021/acs.jpcc.6b01741. URL: https://doi.org/10.1021/acs.jpcc.6b01741.

[15] Ronaldo Rodrigues Pela et al. "Electronic structure of MoS2 revisited: a comprehensive assessment of G0W0 calculations". In: (). to be published.

[16] Kangli Wang and Beate Paulus. "Tuning the binding energy of excitons in the MoS2 monolayer by molecular functionalization and defective engineering". In: *Phys. Chem. Chem. Phys.* 22 (21 2020), pp. 11936–11942. DOI: 10.1039/D0CP01239D. URL: http://dx.doi.org/10.1039/D0CP01239D.

[17] Margherita Marsili et al. "Spinorial formulation of the *GW*-BSE equations and spin properties of excitons in two-dimensional transition metal dichalcogenides". In:

Phys. Rev. B 103 (15 Apr. 2021), p. 155152. DOI: 10.1103/PhysRevB.103.155152. URL: https://link.aps.org/doi/10.1103/PhysRevB.103.155152.

[18] Amall Ramanathan. "2D hexagonal boron nitride for solar energy conversions". In: *PeerJ Materials Science* 5 (Mar. 2023), e27. DOI: 10.7717/peerj-matsci.27.

[19] Dmitrii Nabok, Benjamin Höffling, and Claudia Draxl. *Energy-level alignment at organic/inorganic interfaces from first principles: Example of poly(*para*-phenylene) / rock-salt ZnO(100)*. 2019. arXiv: 1908.07293 [cond-mat.mtrl-sci].

[20] Emilio Artacho et al. "Structural Relaxations in Electronically Excited Poly(*para*-phenylene)". In: *Phys. Rev. Lett.* 93 (11 Sept. 2004), p. 116401. DOI: 10.1103/PhysRevLett.93.116401. URL: https://link.aps.org/doi/10.1103/PhysRevLett.93.116401.

Selbstständigkeitserklärung

Ich erkläre hiermit, dass ich die vorliegende Arbeit selbstständig verfasst und noch nicht für andere Prüfungen eingereicht habe. Sämtliche Quellen einschließlich Internetquellen, die unverändert oder abgewandelt wiedergegeben werden, insbesondere Quellen für Texte, Grafiken, Tabellen und Bilder, sind als solche kenntlich gemacht. Mir ist bekannt, dass bei Verstößen gegen diese Grundsätze ein Verfahren wegen Täuschungsversuchs bzw. Täuschung eingeleitet wird.

Berlin, den 30.12.2023,